Reactive transport modelling with a coupled OpenFOAM®-PHREEQC platform

Saideep Pavuluri*[1], Christophe Tournassat[1,2], Francis Claret[1], and Cyprien Soulaine[1]

[1]Institut des Sciences de la Terre d'Orléans (ISTO), Université d'Orléans, Centre national de la recherche scientifique (CNRS), Bureau de Recherches Géologiques et Minières (BRGM), Orléans, France

[2]Earth and Environmental Sciences Area, Lawrence Berkeley National Laboratory, Berkeley, CA, USA

October 20, 2022

Abstract

Reactive transport modelling has established itself as a key player to analyze sophisticated hydro-geochemical interactions that occur over spatio-temporal scales on par with subsurface applications. In this paper, we benchmarked a new reactive transport package - *porousMedia4Foam* at the continuum-scale considering complex and well established cases available in the reactive transport modelling community. *porousMedia4Foam* was born by the successful coupling of two open-source packages – OpenFOAM® and PHREEQC. The flow governing equations, transport of species and the evolution of porous media properties are handled by OpenFOAM® whereas, the geochemistry is exclusively handled by PHREEQC. We further demonstrated the capability of using *porousMedia4Foam* to investigate reactive transport processes considering unstructured meshes. As *porousMedia4Foam* is an open-source package with included benefits to account for reactive transport processes occurring at various scales – pore-, hybrid-, and, Darcy- scales, we believe that *porousMedia4Foam* opens a new dimension to analyze reactive transport physics for various intriguing subsurface applications.

Keywords: hydrology; geochemistry; reactive transport modelling; code benchmarks; *porousMedia4Foam*; OpenFOAM®; PHREEQC.

1 Introduction

Understanding and predicting the behaviour of fluid flow and reactivity in geological porous media had gathered widespread attention for many decades. Early applications of this knowledge included deciphering groundwater movement and contaminant spreading in aquifers (Bear, 1972) or hydrocarbons movement in

*Corresponding author: saideep025@gmail.com

oil bearing strata (Aziz, 1979; Dake, 1983). More recent applications included the use of the subsurface settings for the storage of energy - e.g. in the form of hydrogen gas (Bauer et al., 2013; Heinemann et al., 2021), or of nuclear and industrial wastes (Landais, 2006; Claret et al., 2018; Bildstein et al., 2019), as well as for the sequestration of carbon dioxide emitted by industries (Lackner, 2003; André et al., 2007; Haszeldine, 2009; DePaolo and Cole, 2013; Trebotich et al., 2014). To decipher the complex interplay between fluid flows and reactivity in subsurface applications, it is necessary to account for the coupled and non-linear processes that include thermal, hydrological, mechanical and chemical (THMC) interactions (Bildstein and Claret, 2015; Zhang et al., 2016; Bea et al., 2016; Soulaine and Tchelepi, 2016; Soulaine et al., 2018; Tournassat and Steefel, 2019; Pavuluri, 2019). Minor changes in THMC parameters at the pore-scale can initiate major changes in other properties influencing the movement of fluids in the subsurface (Noiriel, 2015; Noiriel et al., 2016; Noiriel and Daval, 2017; Molins et al., 2020; Poonoosamy et al., 2020; Soulaine et al., 2021a). For example, the chemical interactions of pore fluids with minerals bordering the pores may either result in dissolution or precipitation processes, which in turn alter physical properties of the porous medium such as porosity, permeability, diffusivity and reactive surface area of minerals (Min et al., 2015; Chagneau et al., 2015a,b; Luhmann et al., 2017; Soulaine et al., 2017; Niu and Zhang, 2019). These parameters govern the nature of fluid flows along with aqueous species reactivity and transport. Therefore, these parameters have a key role in the evaluation of the efficiency and safety for a number of environmental applications. In this respect, fluid flow and chemical reactivity model predictions must take into account spatial heterogeneity, which can be time-dependent in response to physical and chemical perturbations. For this reason, reactive transport modeling (RTM) has extensively been used to comment on the safety, and to provide optimal operational and design strategies for various subsurface applications (Mayer et al., 2002a; Steefel et al., 2005; Gaus et al., 2008; Druhan et al., 2020). The main advantage of RTM is that it integrates both the essential ingredients required to assess the ongoing dynamic processes in subsurface applications – fluid flow and geochemistry. There already exist several reactive transport packages such as TOUGHREACT (Xu et al., 2011), CrunchFlow (Steefel, 2009), MIN3P (Mayer et al., 2002b), PFLOTRAN (Lichtner et al., 2015) amongst others. The review by Steefel et al. (2015) provided an extended description of various reactive transport packages and compared the packages on different grounds such as code availability (i.e. open-/ close-source), possibility to run simulations in parallel, and numerical schemes, along with implemented geochemistry and physical modelling features.

The development of reactive transport packages is a continuous and dynamic task primarily benefiting from, and triggering new research directions on the coupling of basic processes responsible for complex non-linear THMC behaviors (Steefel, 2019). In this respect, the authors recently developed a multi-scale reactive transport open-source package *porousMedia4Foam* (Soulaine et al., 2021b), which included capabilities to model hydro-geochemistry at pore-, continuum-, and, hybrid- scales. *porousMedia4Foam* coupled two well established open-source packages namely, (i) OpenFOAM®, which is used to solve fluid flow, transport of species, and compute evolution of porous media properties such as permeability, reactive surface area of minerals, and (ii) PHREEQC (Parkhurst and Appelo, 2013), which is used to solve for the geochemical interactions. *porousMedia4Foam* can simulate hydro-geochemical processes in complex and heterogeneous geological settings using unstructured meshes, which is a capability available in only a few reactive transport packages like TOUGHREACT (Xu et al., 2011), MIN3P (Su et al., 2020), PFLOTRAN (Lichtner et al., 2015). In addition, *porousMedia4Foam* maintains a generic coupling interface such that other geochemical packages

can also be integrated into the existing code architecture. Soulaine et al. (2021b) already benchmarked the multi-scale solver of *porousMedia4Foam* with test cases describing calcite dissolution at pore- and Darcy-scales. In this numerical benchmark paper, we investigated the robustness of *porousMedia4Foam* continuum-scale predictions, by comparing the results with state-of-the-art reactive transport codes, for published reference benchmark exercises (Xie et al., 2015; Poonoosamy et al., 2018).

In the following Section 2, we present the mathematical models implemented in *porousMedia4Foam* for solving continuum-scale reactive transport, and we describe the flow solvers and geochemical packages used for the study. Then, in Section 3, we describe the cases that we benchmark in this paper for which reference solutions exist. Later, in Section 4, *porousMedia4Foam* simulation results were compared with state-of-the-art reactive transport codes. Finally, we end the paper with concluding remarks.

2 Solving reactive transport problems with *porousMedia4Foam*

We commence this section by briefly describing about the *porousMedia4Foam* package. A more detailed review of the package and its multi-scale modelling capabilities can be found in Soulaine et al. (2021a). Then, we discuss the geochemical package, flow solvers and models used to describe the evolution of porous media properties in response to transient chemical interactions.

2.1 Package description

porousMedia4Foam (Soulaine et al., 2021b) is an open-source (can be downloaded from `https://github.com/csoulain/porousMedia4Foam`) and generic package developed by the authors to solve hydro-geochemical interactions that occur at multiple scales which include the pore-, continuum-, and, hybrid- scales. *porousMedia4Foam* is built on the skeletal framework of OpenFOAM® (`http://www.openfoam.org`) which is used to solve the governing equations describing fluid flow and transport of species. All common models that are used to describe the evolution of permeability, reactive surface area and dispersivities are available as part of the *porousMedia4Foam* package. Chemical interactions are solved with PHREEQC (`https://www.usgs.gov/software/phreeqc-version-3`), using its reaction module PhreeqcRM (Parkhurst and Wissmeier, 2015) which establishes communication between the OpenFOAM® and geochemistry results.

porousMedia4Foam (Soulaine et al., 2021b) is an open-source (can be downloaded from `https://github.com/csoulain/porousMedia4Foam`) and generic package developed by the authors to solve hydro-geochemical interactions that occur at multiple scales which include the pore-, continuum-, and, hybrid- scales. *porousMedia4Foam* is built on the skeletal framework of OpenFOAM® (`http://www.openfoam.org`) which is used to solve the governing equations describing fluid flow and transport of species. Chemical interactions are solved with PHREEQC (`https://www.usgs.gov/software/phreeqc-version-3`). The reaction module PhreeqcRM (Parkhurst and Wissmeier, 2015) is used to establish a communication between the results of OpenFOAM® and PHREEQC.The coupling of OpenFOAM® and PHREEQC is expected to attract users from both communities of research.

porousMedia4Foam can solve for the flow using Darcy-Brinkman-Stokes equation (Soulaine et al., 2021b). When the porosity ϕ is equal to 1, the Navier-Stokes equations is solved. On the other hand, when the porosity ϕ is in-between 0 and 1, the Darcy's equation is solved. Irrespective of the scale under consideration, the chemistry is solved using PHREEQC in the same manner as described in Section 2.2. The usage of this

approach provides an added advantage to use *porousMedia4Foam* for various process engineering applications as well that may include investigating reactive transport processes in pipes and reactors not only restricting the scope of usage to the porous media research community.

porousMedia4Foam is also expected to play a pivotal role in the area of upscaling. *porousMedia4Foam* can assist experimentalists to validate various empirical relations to update/ improve parameters such as the permeability of the medium k. In the current version of *porousMedia4Foam*, all common models that are used to describe the evolution of permeability, reactive surface area and dispersivities are available.

As the focus of this paper is exclusively at the Darcy scale, we have chosen to use the Darcy equation to solve for the flow as we described in Section 2.3. Fig. 1 shows a flowchart that describes how the reactive transport algorithm in *porousMedia4Foam* works in a time step. A more detailed explanation regarding each block mentioned in Fig. 1 is described in the sub-sections 2.2, 2.3, and, 2.4.

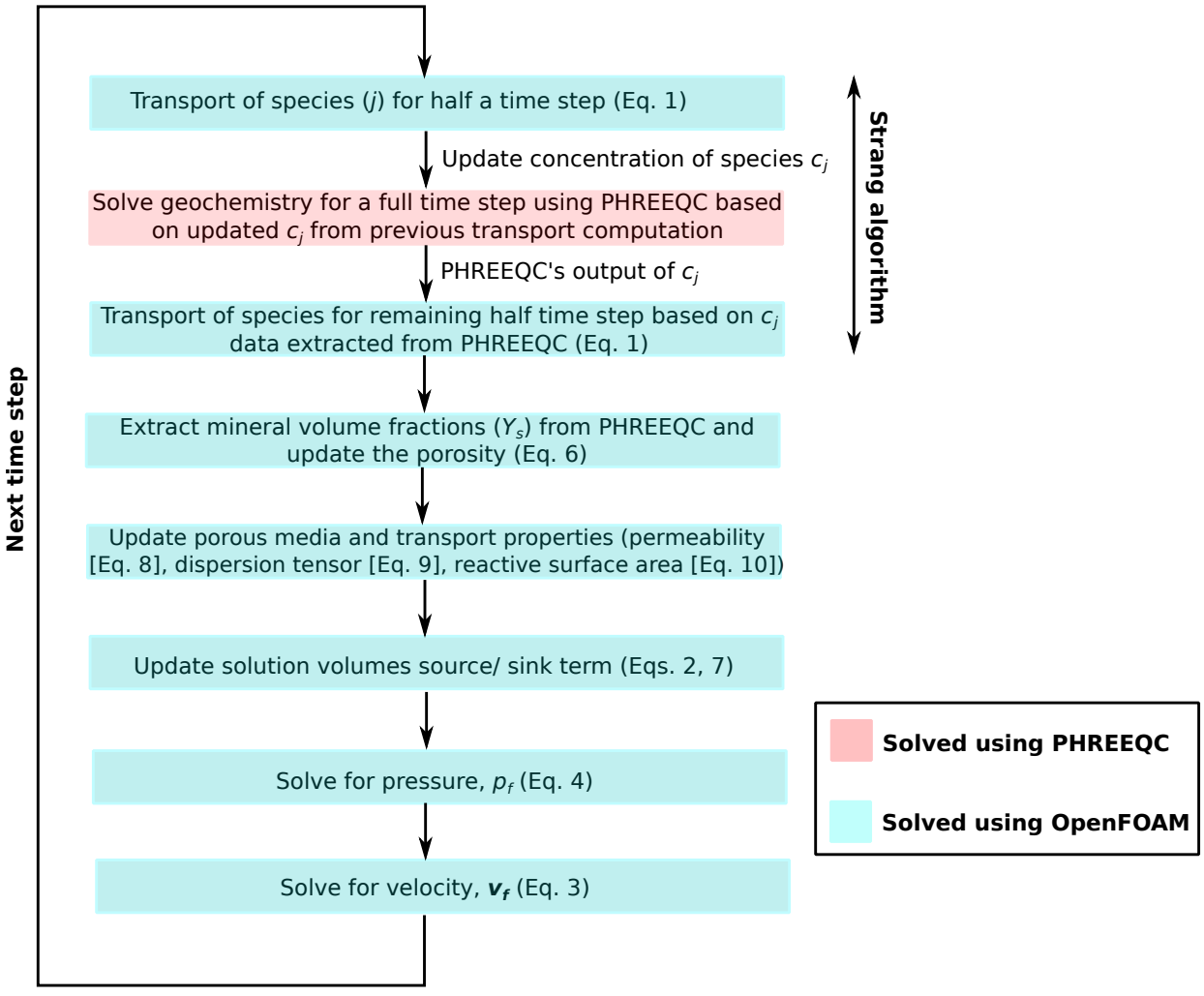


Figure 1: Flowchart describing various steps followed in a time step to solve hydro-geochemical problems using *porousMedia4Foam*

.

2.2 Geochemical package - phreeqcRM

In *porousMedia4Foam*'s geochemical package phreeqcRM, the coupling between transport of species and chemistry relies on the operator-splitting strategy. Within a time-step, the transport of species is solved without reaction using the finite-volume method embedded in OpenFOAM, and the geochemical reactions are computed using PHREEQC without transport. The PhreeqcRM module transfers essential information such as the concentration of species and minerals between the flow solver and the geochemical solver PHREEQC.

The transport of species j having concentration C_j is performed according to the following advection-diffusion equation,

$$\frac{\partial \phi C_j}{\partial t} + \nabla \cdot (\boldsymbol{v}_f C_j) - \nabla \cdot (\phi D^* \nabla C_j) = 0. \tag{1}$$

In the above equation, ϕ is the porosity, $\boldsymbol{v}_f$ is the fluid velocity determined by the flow solver and D^* is the effective diffusion coefficient that accounts for tortuosity and hydrodynamic dispersion.

The transport of species is followed by solving for the chemistry using PHREEQC. The geochemical package updates the solution composition C_j and the distribution of solid minerals $Y_{s,i}$. It is possible to account for phase equilibrium and/ or kinetically controlled reactions. For the later, reactive surface areas of minerals A_e must be defined.

Strang's algorithm (Strang, 1968) which has second order accuracy (Carrayrou et al., 2004) is used for operator-splitting. First, species transport (Eq. 1) is carried out for half a time step. Second, chemistry is solved for an entire time step, using updated species concentrations C_j. Lastly, the transport equation is once again solved for the remaining half time step.

2.3 Flow solvers

porousMedia4Foam comprises of three flow solvers: 1. constantVelocityFoam - a solver that uses specified velocity field within the system; 2. darcyFoam - a continuum-scale solver based on Darcy's law and; 3. dbsFoam - a multi-scale solver based on Darcy-Brinkman-Stokes formulation (Soulaine et al., 2021b). For the continuum-scale benchmark cases discussed in this paper, we either used the darcyFoam or the constantVelocityFoam flow solvers.

darcyFoam is a standard continuum-scale solver for Darcy's law (Darcy, 1856). Considering a reactive environment comprising of an incompressible fluid having density ρ_f and N_s number of minerals, the continuity equation considering mineral dissolution (mineral convert to solution)/ precipitation (solution convert to mineral) is given by,

$$\nabla \cdot \boldsymbol{v}_f = \sum_{i=1}^{N_s} \dot{m}_{s,i} \left(\frac{1}{\rho_f} - \frac{1}{\rho_{s,i}} \right), \tag{2}$$

where $\rho_{s,i}$ is the density of mineral i and $\dot{m}_{s,i}$ is the rate of mass transfer of solid to solution or vice-versa obtained from the geochemistry computations (Eq. 7). Darcy's law used to describe single-phase flow in porous media at the continuum-scale is given by,

$$\boldsymbol{v}_f = -\frac{k}{\mu_f} \left(\nabla p_f - \rho_f \boldsymbol{g} \right), \tag{3}$$

where k is the permeability of the medium, μ_f is the fluid viscosity, ∇p_f is the pressure gradient, and, $\boldsymbol{g}$

is the acceleration due to gravity. Combining the continuity equation (Eq. 2) and the Darcy's law (Eq. 3) results in the following Laplace equation for the pressure p_f which is solved implicitly,

$$-\nabla \cdot \frac{k}{\mu_f} \nabla p_f + \nabla \cdot \rho_f \mathbf{g} = \sum_{i=1}^{N_s} \dot{m}_{s,i} \left(\frac{1}{\rho_f} - \frac{1}{\rho_{s,i}} \right). \tag{4}$$

The modelling domain is discretized using a finite-volume method and a sequential approach is used to solve the flow governing equations. Once the pressure field is computed, the velocity is determined using Eq. 3. Fixed values for pressure and velocity can be specified at the boundaries. However, as the pressure field is solved implicitly, the fixed value boundary conditions defined for velocity are transformed into a pressure gradient boundary defined by darcyGradPressure (Horgue et al., 2015) in *porousMedia4Foam*. According to the Darcy's law, pressure gradient normal to the domain boundary $\boldsymbol{n} \cdot \nabla p_f$ is given by,

$$\boldsymbol{n} \cdot \nabla p_f = -\boldsymbol{n} \cdot \left(\mu_f k^{-1} \boldsymbol{v}_f - \rho_f \boldsymbol{g} \right). \tag{5}$$

constantVelocityFoam is a steady-state flow solver with the fluid velocity $\boldsymbol{v}_f$ defined for each control volume within the domain. For example, the velocity data can be an output from a separate flow simulation or can be a data specified by the user. The velocity can either be uniform or non-uniform. This solver is particularly useful when geochemical interactions have a negligible influence on fluid flow.

2.4 Evolution of porous media properties: principles and equations

In this section, we present the mathematical models that describe the evolution of porous media properties such as porosity ϕ, permeability k, dispersivity D^* and reactive surface area A_e. Apart from the standard models described below, additional models that describe the evolution of porous media properties which are available in *porousMedia4Foam* can be found in Soulaine et al. (2021b).

2.4.1 Minerals distribution and porosity

Porosity ϕ defines the volumetric ratio of pore volume in a porous material that contain N_s solid minerals in the solid matrix. Each of these minerals occupy a volume fraction of $Y_{s,i}$. During hydro-geochemical interactions, mineral precipitation and dissolution result in porosity variations. In *porousMedia4Foam*, it is possible to maintain a constant porosity or update the porosity due to ongoing geochemical interactions according to,

$$\phi = 1 - \sum_{i}^{N_s - 1} Y_{s,i} - Y_{s,\text{inert}}, \tag{6}$$

where $Y_{s,\text{inert}}$ refers to the constant volume fraction of inert minerals.

The rate of solid mass change (caused due to mineral dissolution/ precipitation), $\dot{m}_{s,i}$, used as a source/ sink term in the continuity equation (Eq. 2) is computed as,

$$\dot{m}_{s,i} = -\frac{\partial \rho_{s,i} Y_{s,i}}{\partial t}. \tag{7}$$

2.4.2 Evolution of permeability, dispersivity and reactive surface area

In continuum-scale models, properties such as permeability k and dispersivity D^* are dependent on porosity ϕ, and reactive surface area of minerals A_e are dependent on individual minerals volume fraction $Y_{s,i}$. Corresponding relationships have been established empirically (Xie et al., 2015; Poonoosamy et al., 2018).

The permeability k present in Darcy's equation (Eq. 3) influences the fluid flow velocity. The evolution of permeability as a function of porosity is commonly described according to the Kozeny-Carman equation (Kozeny, 1927; Carman, 1937):

$$k = k_0 \left(\frac{\phi}{\phi_0} \right)^n \left(\frac{1-\phi_0}{1-\phi} \right)^m. \tag{8}$$

where k_0 refers to the initial permeability, n and m are user-defined empirical exponents, which are specific to the investigated materials and hydrodynamic conditions, and ϕ_0 is the initial porosity of the medium.

The dispersion coefficient D^* in Eq. 1 is a parameter that governs the spreading of chemical species in the porous medium. The dispersion of species is computed using a linear dispersion model:

$$D^* = \phi^n D \left(1 + \frac{\alpha_L}{D} |\boldsymbol{v}_f| \right), \tag{9}$$

where ϕ^n represents the effects of tortuosity according to Archie's law (Archie, 1942), D is a molecular diffusion coefficient, α_L is the lateral dispersion coefficient.

Reactive surface area of minerals $A_{e,i}$ are needed to compute the results of kinetic rate laws. The reactive surface area of all minerals (primary and secondary) can be updated in *porousMedia4Foam* according to a power-law model (Xie et al., 2015; Poonoosamy et al., 2018):

$$A_{e,i} = A_{0,i} (Y_{s,i})^n, \tag{10}$$

where $A_{0,i}$ is the initial reactive surface area of minerals, $Y_{s,i}$ is the volume fraction of minerals and n is a user-defined exponent.

3 Description of case studies

porousMedia4Foam results were verified by comparison with continuum-scale benchmarks published in the literature. Table 1 provides a brief summary of all the cases investigated in this benchmark study. The investigated cases are presented in increasing levels of complexity. All input files required to run the test cases in Table 1 are available as examples in the *porousMedia4Foam* package.

Cases 1a,b and 2 considered mineral dissolution and precipitation in a one-dimensional (1D) domain. Calcite dissolution was modelled using thermodynamic equilibrium conditions and kinetic reactions in cases 1a and 1b respectively. Case 2 involved multiple minerals in which, calcite dissolution was described using kinetic reaction rates, while dolomite precipitation/dissolution was modelled using thermodynamic local equilibrium. In both cases (case 1 and 2), porosity feedback on transport properties was neglected. Results were compared with reference solutions obtained with PHREEQC TRANSPORT capability. PHREEQC's chemical database *phreeqc.dat* was used for these cases.

Cases 3 to 7 reproduced 5 benchmarks of varying complexity, which were run with reactive transport

Case	Dim.	Porosity feedback	Kin. reac.	Phase equ.	Comments: considering	Comparison with
1a	1D	no		yes	ADS, mineral dissolution	PHREEQC results
1b	1D	no	yes		ADS, mineral dissolution	PHREEQC results
2	1D	no	yes	yes	ADS, evolution of multiple (2) minerals	PHREEQC results
3	1D	yes	yes		AS, mineral dissolution	Bench. 1 in Xie et al. (2015)
4	1D	yes	yes		AS, evolution of multiple (2) minerals, clogging	Bench. 2 in Xie et al. (2015)
5	1D	yes	yes		AS, multiple (6) minerals evolution, redox reactions, clogging	Bench. 3 in Xie et al. (2015)
6	1D	yes	yes		ADS, multiple minerals (6) evolution, redox reactions, clogging	Bench. 5 in Xie et al. (2015)
7	2D	yes	yes		ADS, multiple minerals (6) evolution, redox reactions, clogging	Bench. 6 in Xie et al. (2015)
8	2D	yes	yes	yes	Evolution of mineral having different grain sizes	Bench. 3a in Poonoosamy et al. (2018)

Table 1: Summary of the benchmark cases simulated with *porousMedia4Foam*. ADS refers to an advective diffusive system and AS refers to an advective system.

codes presented in Xie et al. (2015): CrunchFlow, HP1, MIN3P, PFlotran and TOUGHREACT. For the sake of simplicity and to ensure figure readability, we only showed MIN3P and TOUGHREACT results for comparison, but readers can refer to Xie et al. (2015) for comparison of results with other reactive transport codes. In these case studies primary minerals were calcite, gibbsite and siderite whereas secondary minerals were jarosite, ferrihydrite and gypsum. Porous media properties were updated at run time according to mineral dissolution/precipitation reactions, which were described using kinetic reaction rates only. For these benchmarks, we used the chemical database provided in Xie et al. (2015).

Case 8 was a two-dimensional (2D) case based on the numerical benchmark of Poonoosamy et al. (2018) in which celestite with a bimodal grain size distribution reacted with barium chloride solution, leading to barite precipitation and celestite dissolution. Geochemical reactions were described using kinetic rates (for celestite) and thermodynamic local equilibrium (for barite), according to *PSI/Nagra* chemical thermodynamic database (Thoenen et al., 2014). Porous media properties were updated at run time according to mineral dissolution/precipitation reactions.

3.1 Cases 1a and 1b: Calcite dissolution — no porosity feedback

A 1D porous column of length 0.5 m was uniformly filled with 57 % of an inert mineral and with 3 % of calcite. An acidic solution at pH 2 was continuously injected from the inlet boundary at a constant rate of $10^{-4}\,\mathrm{m}^3/\mathrm{s}$. Initial conditions and description of the primary components continuously injected into the system are provided in Table 2. In such a reactive setup, the dissolution of calcite occurs according to:

$$\begin{aligned} \mathrm{CaCO_3} + \mathrm{H^+} &\leftrightarrow \mathrm{Ca^{2+}} + \mathrm{HCO_3^-}, \\ \mathrm{HCO_3^-} &\leftrightarrow \mathrm{H^+} + \mathrm{CO_3^{2-}}. \end{aligned} \tag{11}$$

In case 1b, calcite dissolution rate constant was $k_{\mathrm{calcite}} = 1\,\mathrm{mol/m^2/s}$, and calcite reactive surface area was $A_0 = 1\,\mathrm{m^2/m^3_{mineral}}$. For cases 1a,b evolution of transport parameters such as porosity, permeability and reactive surface area due to mineral reactivity were neglected and we used `constantVelocityFoam` – the *porousMedia4Foam* flow solver (Section 2.3). The transport of species was modeled using Eq. 1. For the dispersion model (Eq. 9), the molecular diffusion coefficient was $D = 10^{-9}\,\mathrm{m^2/s}$, hydrodynamic dispersion coefficient $\alpha_L = 10^{-4}\,\mathrm{m}$, and an exponent $n = 0$. The spatial domain was discretized using 50 cells (each

cell 10 mm long). We followed the evolution of calcite volume fraction and primary ion concentrations for one hour of reaction time. The results for this case are discussed in Section 4.1.

Primary components	Units	Initial condition	Injected solution
pH	-	8.2	2
Ca^{2+}	mol/L	5.113×10^{-4}	0
CO_3^{2-}	mol/L	1.018×10^{-3}	0
Cl^-	mol/L	9.97×10^{-16}	10.95×10^{-3}

Table 2: Cases 1a and 1b – Initial conditions and description of primary components injected for calcite dissolution considering thermodynamic local equilibrium and kinetics.

3.2 Case 2: Calcite dissolution and dolomite precipitation/ dissolution — no porosity feedback

In case 2, conditions were similar to case 1b (calcite dissolution based on kinetics), except that the injected solution also contained magnesium (Mg^{2+}). Dolomite $\left(CaMg(CO_3)_2\right)$ was allowed to precipitate and to dissolve at thermodynamic local equilibrium according to:

$$CaMg(CO_3)_2 + 2H^+ \leftrightarrow Ca^{2+} + Mg^{2+} + 2HCO_3^-. \tag{12}$$

Initial conditions and description of the primary components continuously injected into the system are provided in Table 3. We followed the evolution of mineral volume fractions and primary ions within the system for one hour and the results are discussed in Section 4.2.

Primary components	Units	Initial conditions	Injected solution
pH	-	8.2	2
Ca^{2+}	mol/L	5.113×10^{-4}	0
Mg^{2+}	mol/L	0	9.967×10^{-3}
CO_3^{2-}	mol/L	1.018×10^{-3}	0
Cl^-	mol/L	9.97×10^{-16}	31.51×10^{-3}

Table 3: Case 2 – Initial conditions and description of the primary components injected for the case of calcite dissolution - dolomite precipitation/ dissolution.

3.3 Case 3: Advective system subjected to porosity opening - Calcite dissolution and porosity feedback on permeability

In case 3, we verified the ability of *porousMedia4Foam* to simulate coupled hydro-geochemical processes that included porosity feedback on transport properties and we used darcyFoam - the *porousMedia4Foam* flow solver (Section 2.3). Case 3 corresponds to Benchmark 1 described in Xie et al. (2015). It consisted of a 2 meters long 1D column initially filled with 35 % of inert mineral and 30 % of calcite. An acidic solution at pH 3 was injected at the inlet to initiate the dissolution of calcite (Eq. 11). The kinetic reaction rate constant of calcite was $k_{\text{calcite}} = 5 \times 10^{-5}\,\text{mol/m}^2\text{/s}$ and initial reactive surface area was $A_0 = 1\,\text{m}^2/\text{m}^3_{\text{mineral}}$. The reactive surface area evolved according to the power law function (Eq. 10) with $n = 2/3$. According to the

volume fraction of calcite dissolved, the porosity was updated at run time following Eq. 6. Table 4 provides the initial conditions and a description of primary components injected continuously into the system. A

Primary components	Units	Initial conditions	Injected solution
pH	-	9.38	3
Ca^{2+}	mol/L	1.56×10^{-4}	9.97×10^{-5}
CO_3^{2-}	mol/L	2.56×10^{-4}	9.97×10^{-3}
SO_4^{2-}	mol/L	9.97×10^{-11}	6.44×10^{-4}

Table 4: Case 3 – Initial conditions and description of the primary components injected for calcite dissolution under kinetic conditions considering porosity feedback.

hydraulic head of 0.007 m was applied between the inlet and outlet (Xie et al., 2015) by fixing the inlet pressure at 70 Pa and the outlet pressure at 0 Pa. The species were transported only due to advection (in Eq. 1, $D^* = 0$). The permeability evolved according to Kozeny-Carman relation (Eq. 8) where the initial permeability was $k_0 = 1.186 \times 10^{-11}\,\mathrm{m}^2$, $m = 2$ and $n = 3$. The domain was spatially discritized using 80 cells (each cell 25 mm long). We tracked the evolution of calcite volume fraction and other porous media properties for 150 years of reaction time. The results for this case are discussed in Section 4.3.

3.4 Case 4: Advective system subjected to porosity clogging - Calcite dissolution, gypsum precipitation/ dissolution and porosity feedback on permeability

Case 4 corresponds to Benchmark 2 in Xie et al. (2015). The setup was the same as in case 3 (calcite dissolution based on kinetics, Section 3.3) except that an acidic solution containing sulfate ions (SO_4^{2-}) was injected through the system resulting in the precipitation/ dissolution of gypsum ($CaSO_4.2H_2O$):

$$CaSO_4.2H_2O \leftrightarrow Ca^{2+} + SO_4^{2-} + 2H_2O. \tag{13}$$

Table 5 provides the initial composition and the solution continuously injected into the system. As the molar

Primary components	Units	Initial conditions	Injected solution
pH	-	9.33	3
Ca^{2+}	mol/L	1.69×10^{-4}	9.97×10^{-5}
CO_3^{2-}	mol/L	2.69×10^{-4}	9.97×10^{-3}
SO_4^{2-}	mol/L	1.69×10^{-4}	0.2
Na^{+}	mol/L	3.19×10^{-4}	0.394

Table 5: Case 4 – Initial conditions and description of the primary components injected for calcite dissolution and gypsum precipitation/ dissolution under kinetic conditions considering porosity feedback.

volume of gypsum, $V_{\mathrm{m,gypsum}} = 74.21\times10^{-6}\,\mathrm{m}^3/\mathrm{mol}$, is twice that of calcite, $V_{\mathrm{m,calcite}} = 36.93\times10^{-6}\,\mathrm{m}^3/\mathrm{mol}$, precipitation of gypsum was expected to clog the porosity. For gypsum, the kinetic reaction rate was $k_{\mathrm{gypsum}} = 5 \times 10^{-5}\,\mathrm{mol/m^2/s}$ and the initial reactive surface area was $A_0 = 1\,\mathrm{m}^2/\mathrm{m}^3_{\mathrm{mineral}}$. The reactive surface area for gypsum evolved according to Eq. 10 with $n = 1$. Chemical species were transported by advection only (in Eq. 1, $D^* = 0$). 150 years of transport and geochemical reactions were simulated and the results are discussed in Section 4.4.

3.5 Case 5: An advective system with complex geochemical reactions and porosity feedback on permeability

Case 5 corresponds to Benchmark 3 in Xie et al. (2015). A one-dimensional 2 m long column was filled with 22 % calcite, 5 % siderite, 5 % gibbsite and 33 % of an inert mineral. The initial composition and solution continuously injected into the system is shown in Table 6. The pressure was fixed at 70 Pa at the inlet and

Primary components	Units	Initial conditions	Injected solution
pH	-	8.01	3
Ca^{2+}	mol/L	4.74×10^{-4}	9.97×10^{-5}
CO_3^{2-}	mol/L	2.14×10^{-3}	9.97×10^{-3}
SO_4^{2-}	mol/L	1.69×10^{-4}	0.1
Na^{+}	mol/L	1.49×10^{-3}	0.09
Al^{3+}	mol/L	2.8×10^{-7}	1.43×10^{-2}
K^{+}	mol/L	9.97×10^{-6}	7.65×10^{-5}
Fe^{2+}	mol/L	6.59×10^{-6}	1.14×10^{-8}
Fe^{3+}	mol/L	2.53×10^{-8}	2.23×10^{-2}

Table 6: Initial conditions and description of the primary components injected in cases 5-7.

at 0 Pa at the outlet. The presence of aluminum (Al^{3+}), potassium (K^{+}), ferrous (Fe^{2+}) and ferric (Fe^{3+}) ions resulted in the formation of ferrihydrite, jarosite, gibbsite and siderite within the system according to the following reactions:
Ferrihydrite:

$$Fe^{3+} + 3H_2O \leftrightarrow Fe(OH)_3 + 3H^{+}, \tag{14}$$

Jarosite:

$$K^{+} + 3Fe^{3+} + 2SO_4^{2-} + 6H_2O \leftrightarrow KFe_3(SO_4)_2(OH)_6 + 6H^{+}, \tag{15}$$

Gibbsite:

$$Al^{3+} + 3H_2O \leftrightarrow Al(OH)_3 + 3H^{+}, \tag{16}$$

and Siderite:

$$Fe^{2+} + CO_3^{2-} \leftrightarrow FeCO_3. \tag{17}$$

All the above reactions were described using the kinetic reaction rates $k_{\text{calcite}} = k_{\text{gypsum}} = 5\times10^{-5}$ mol/m^2/s, $k_{\text{gibbsite}} = 5\times10^{-7}$ mol/m^2/s and $k_{\text{ferrihydrite}} = k_{\text{jarosite}} = k_{\text{siderite}} = 5\times10^{-6}$ mol/m^2/s. The initial reactive surface area for all minerals was $A_0 = 1\,\text{m}^2/\text{m}^3_{\text{mineral}}$. The reactive surface area of minerals evolved as a function of the individual mineral content using a power-law, with $n = 2/3$ (Eq. 10) for calcite, gibbsite and siderite, and with $n = 1$ for other minerals. Chemical species were transported by advection only (in Eq. 1, $D^* = 0$). The permeability evolved according to the Kozeny-Carman relationship (Eq. 8) with $k_0 = 1.186\times10^{-11}\,\text{m}^2$, $m = 2$, and $n = 3$. The column was spatially discretized using 80 cells (each cell 25 mm long). 300 years of hydro-geochemical interactions were simulated and the results are discussed in Section 4.5.

3.6 Case 6: An advective-diffusive system with complex geochemical reactions and porosity feedback on permeability

The objective of case 6 was to verify the ability of *porousMedia4Foam* to simulate complex geochemical reactions in an advective-diffusive system. It was based on the Benchmark 5 in Xie et al. (2015). The case setup was similar to case 5 (for kinetic reaction rates, evolution of reactive surface area of all minerals and permeability, see Section 3.5) with the notable exception of the presence of diffusive effects modelled using Eq. 9 with $D = 10^{-9}\,\mathrm{m}^2/\mathrm{s}$, $n = 1/3$ and $\alpha_L = 0\,\mathrm{m}$. 300 years of reactive transport had been simulated and the results for this case are presented in Section 4.6.

3.7 Case 7: A 2D advective-diffusive system with complex geochemical reactions and porosity feedback on permeability

This case was based on Benchmark 6 in Xie et al. (2015) and aimed at demonstrating the ability of RTM to model complex two-dimensional systems including comprehensive reaction networks and advective-diffusive transport. The chemical system – solid minerals, aqueous solution composition, geochemical reactions – and the transport model describing this case was similar to case 6 (Section 3.6). The computational domain consisted a 2D system of dimensions 3 m in length and 2 m in height discretized with cells having $\Delta x = 100\,\mathrm{mm}$ and $\Delta y = 50\,\mathrm{mm}$ (30×40 cells). The initial permeability field was heterogeneous as shown in Fig. 2. The permeability for *porousMedia4Foam* simulation (Fig. 2) was defined at the cell centres using linear interpolation of nodal data of permeability provided in Xie et al. (2015). P1, P2 in Fig. 2 indicate the points at which the porosity, permeability data were followed. 300 years of reactive transport was simulated and the results are discussed in Section 4.7.

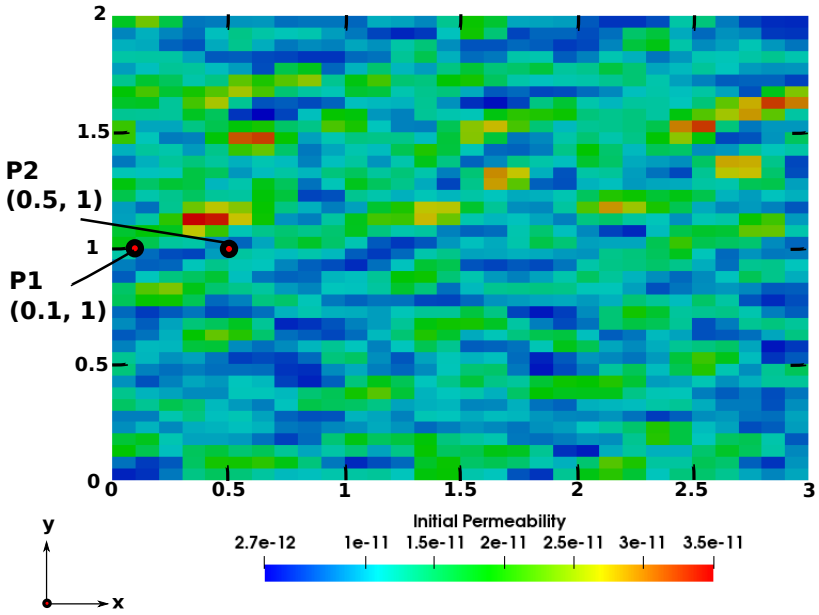


Figure 2: Case 7 – Initial heterogeneous permeability field profile. Points P1 and P2 indicate the location where the porosity had been sampled in Fig. 12.

3.8 Case 8: Reactive zone comprising of celestite having different grain sizes and considering porosity feedback on permeability

In this case, we investigated reactive transport occurring in a 2D flow cell containing celestite ($SrSO_4$) having a bimodal grain size distribution. The setup was discussed in detail in Poonoosamy et al. (2018) and is illustrated in Fig. 3a. The flow cell comprised of three compartments - Q1, Q2 and Q3. Q1 and Q3 were composed of inert mineral (quartz). Q2 comprised of a reactive mineral, celestite. ~~An acidic solution~~ The solution comprising of barium (Ba^{2+}) and chloride (Cl^-), was injected continuously from the inlet at a constant rate. Specifics of the solution being injected into the flow cell and the initial solutions composition in the flow cell can be seen in the electronic annex. Once the barium ions reached the reactive zone Q2 in the flow cell, celestite dissociated into strontium (Sr^{2+}) and sulphate (SO_4^{2-}) ions. The barium ions reacted with sulphate ions resulting in the precipitation of barite ($BaSO_4$) according to the following reaction:

$$Ba^{2+} + SrSO_4 \rightarrow BaSO_4 + Sr^{2+}. \tag{18}$$

As barite has a greater molar mass ($V_{\mathrm{m,barite}} = 52.09 \times 10^{-6}\,\mathrm{m^3/mol}$) compared to celestite ($V_{\mathrm{m,celestite}} = 46.38 \times 10^{-6}\,\mathrm{m^3/mol}$), the geochemical reactions would result in reduction of porosity. The dissolution of celestite was taken into account based on kinetics while the formation of secondary minerals (barite, witherite, strontianite etc) relied on thermodynamic equilibrium. In the modelling, celestite grains of different size were treated as two separate minerals. Initially, on the one hand, smaller celestite grains volume fraction and reactive surface area were 0.223 and $A_{\mathrm{celestite,small,0}} = 20000\,\mathrm{m^2/m^3_{mineral}}$, respectively. On the other hand, the volume fraction of larger celestite grains was 0.447 and their reactive surface area was $A_{\mathrm{celestite,large,0}} = 100\,\mathrm{m^2/m^3_{mineral}}$. The reactive surface area of celestite evolved as a linear function of celestite's mineral content (power-law with $n = 1$, Eq. 10). The permeability-porosity relationship was described using Kozeny-Carman law (Eq. 8). The initial permeability of Q1 and Q3 zones was $k = 1.82 \times 10^{-11}\,\mathrm{m^2}$ and for the Q2 zone it was $k = 1.8 \times 10^{-14}\,\mathrm{m^2}$. The exponents m, n in Eq. 8 were set to 2, 3 respectively. The species transport was modelled using a linear dispersion law (Eq. 9) with $D = 10^{-9}\,\mathrm{m^2/s}$, $\alpha_L = 10^{-5}\,\mathrm{m}$ and $n = 1$.

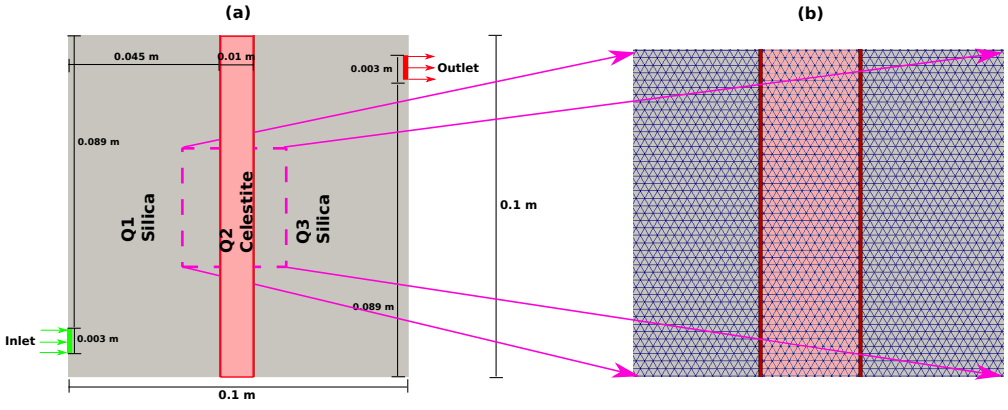


Figure 3: Case 8 – (a) Schematic of the flow cell. (b) Zoom of a section of the flow cell meshed with unstructured triangulated mesh.

The spatial domain was discretized using a Cartesian mesh with $\Delta x = \Delta y = 1\,\mathrm{mm}$ resulting in a total

of 10000 cells. Further, we also ran this benchmark study considering unstructured (triangulated) mesh to show the modelling capabilities of *porousMedia4Foam*. Fig. 3b shows a zoom of a section of the flow domain with the triangular meshes. For this scenario, the domain comprised of 31854 cells. We followed the reactive transport processes for 300 hours and the results are discussed in Section 4.8. Data regarding initial conditions and solution injected into the system can be found in Poonoosamy et al. (2018).

4 Benchmarks results

In this section we discuss and compare the results of *porousMedia4Foam* with other state-of-the-art reactive transport codes for the cases described in Section 3.

4.1 Results of cases 1a and 1b: Calcite dissolution — no porosity feedback

The setup for this case was discussed in Section 3.1. Fig. 4a,b show the results of *porousMedia4Foam* and PHREEQC TRANSPORT module for the evolution of calcite volume fraction and primary species (Cl^-, CO_3^{2-} and Ca^{2+}) for the thermodynamic equilibrium case at time t = 20 min, 40 min and 60 min. As an acidic solution is being continuously injected into the system, calcite dissolves according to Eq. 11. Hence, we noticed the calcite volume fraction front moving towards the outlet (from left to right) over time (Fig. 4a). Subsequently, the dissolution of calcite released CO_3^{2-} and Ca^{2+} into the system (Fig. 4b). As Cl^- is not taking part in any reaction its concentration remained constant throughout the run. Overall, *porousMedia4Foam* is able to capture accurately the behaviour determined by PHREEQC TRANSPORT module.

Fig. 4c,d show the evolution of calcite volume fraction and primary ion concentrations (Cl^-, CO_3^{2-} and Ca^{2+}) along the column length at t = 20 min, 40 min and 60 min when geochemical processes are treated using kinetic reactions (case 1b). Essential data required to describe kinetic rate law for this case is specified in Section 3.1. The ongoing geochemical processes in the system were similar to the previous case (case 1a) except that the dissolution rate of calcite was governed by the kinetic rate law. We found a very good match between the results of *porousMedia4Foam* coupled with PhreeqcRM and the reference solution calculated using PHREEQC and its TRANSPORT module.

4.2 Results of case 2: Calcite dissolution and dolomite precipitation/ dissolution - no porosity feedback

The setup for this case was discussed in Section 3.2. Fig. 5a show the evolution of the mineral volume fractions – calcite and dolomite determined by *porousMedia4Foam* and PHREEQC along the length of the column at time t = 20 min, 40 min and 60 min. Fig. 5b,c show the results of primary ions (Ca^{2+}, Mg^{2+}, Cl^-, and CO_3^{2-}) concentration determined by the packages at different time intervals (t =20 min, 40 min and 60 min) along the column. As the acidic solution is injected into the system, calcite started to dissolve (Eq. 11) releasing carbonate ions into the system. The injected magnesium in presence of carbonate ions reacted to precipitate dolomite (Eq. 12). Then, as the acidic solution is continuously injected into the system, the precipitated dolomite also dissociated over time in presence of H^+ according to Eq. (12). Overall, from

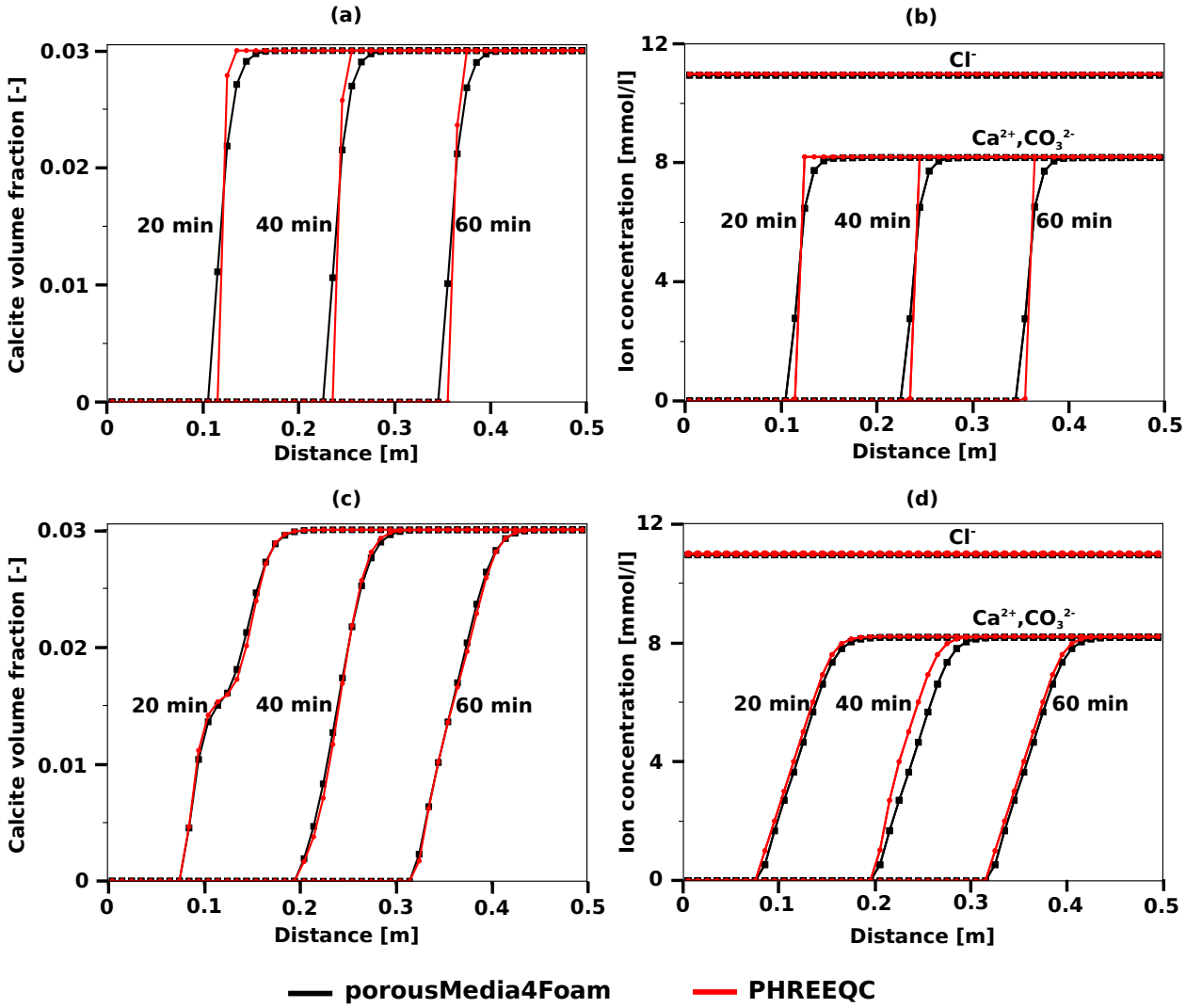


Figure 4: Case 1a/b – Calcite dissolution in a 1D column considering no porosity feedback. Primary ions are Cl^-, CO_3^{2-} and Ca^{2+}. (a) Evolution of calcite volume fraction - considering thermodynamic local equilibrium (case 1a), (b) evolution of primary ion concentrations - considering thermodynamic local equilibrium (case 1a). (c) Evolution of calcite volume fraction - considering kinetic reactions (case 1b), and (d) evolution of primary ion concentrations - considering kinetic reactions (case 1b). In the plot, the *porousMedia4Foam* markers (black squares) and PHREEQC markers (red circles) represent the cell center data.

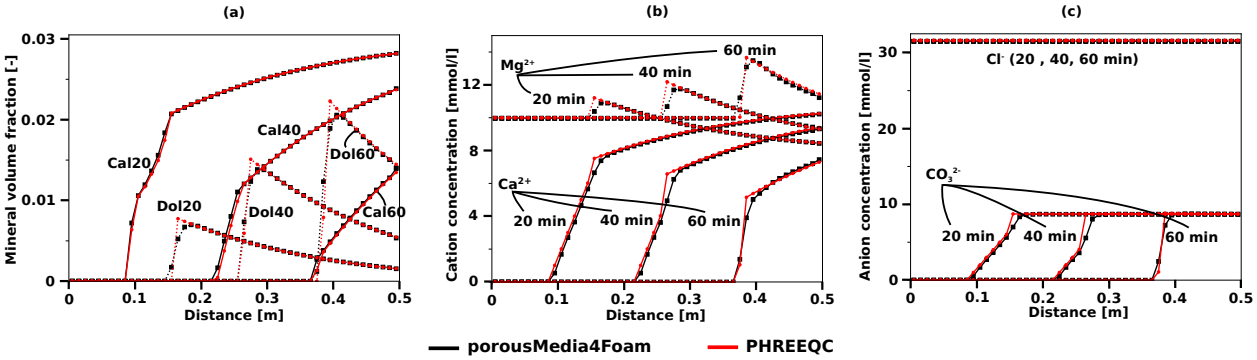


Figure 5: Case 2 – Calcite dissolution and dolomite precipitation/ dissolution in a 1D column considering no porosity feedback. Primary ions are Ca^{2+}, Mg^{2+}, Cl^{-}, and CO_3^{2-}. (a) Evolution of calcite (Cal) and dolomite (Dol) volume fractions. Cal20 refers to calcite volume fraction at $t = 20$ minutes. (b) Evolution of cation (Ca^{2+}, Mg^{2+}) concentrations. (c) Evolution of anion (Cl^{-}, and CO_3^{2-}) concentrations. The markers (black squares for *porousMedia4Foam*, red circles for PHREEQC) represent cell center data collected for both solvers.

Fig. 5a,b,c we noticed a very good match between the results of OpenFOAM coupled with PhreeqcRM and the reference solution calculated using PHREEQC with its TRANSPORT module.

4.3 Results of case 3: Advective system subjected to porosity opening - Calcite dissolution and porosity feedback on permeability

Calcite dissolution was modelled using a kinetic rate of reaction with the data specified in Section 3.3. The ongoing chemical processes were similar to case 1b discussed in Section 4.1 with the notable exception of evolving porous media properties caused due to the change in porosity. In Fig. 6, we compared the results of our hydro-geochemical package *porousMedia4Foam* with other packages – MIN3P and TOUGHREACT. The analysis of results included the evolution of porosity (Fig. 6a), calcite volume fraction (Fig. 6b), hydraulic head (Fig. 6c) along the column length and the outflux over time (Fig. 6d). While computing outflux, we consider column surface area of $1\,m^2$ to be consistent with the benchmark presented in Xie et al. (2015). As the dissolution of calcite occurred, the calcite volume fraction decreased and the porosity increased over time. Consequently, in Fig. 6c, we noticed different slopes of hydraulic head at different times. The slope was minimal where porosity was large and vice-versa. The velocity – and therefore the outflux – increased over time as the permeability (and porosity) of the system increased. The evolution of porosity, calcite volume fraction, hydraulic head and outflux predicted by *porousMedia4Foam* were in close agreement with those of MIN3P and TOUGHREACT which demonstrated the ability of *porousMedia4Foam* to simulate hydro-geochemical processes with porosity feedback. As calcite dissolution reached the end of the column, however, there was a slight difference in the results of *porousMedia4Foam* compared with other solvers. This numerical artefact due to boundary effects was also observed amongst different solvers in the benchmark of Xie et al. (2015) when there was a breakthrough. At 150 years, there was only non reactive inert mineral in the column and the flow reached steady-state.

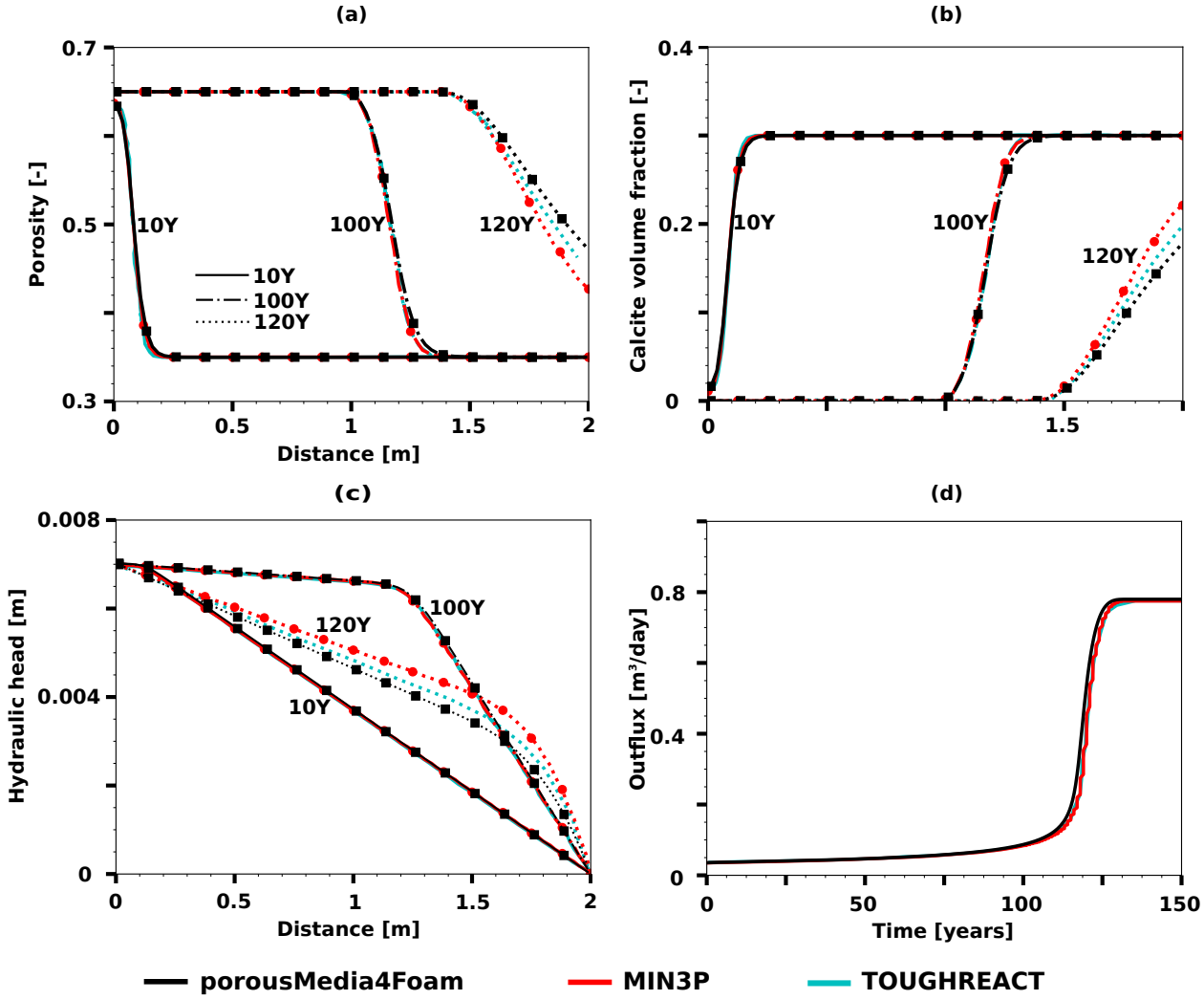


Figure 6: Case 3 - Calcite dissolution under kinetic conditions considering feedback of porous media properties. Evolution of (a) porosity, (b) calcite volume fraction, (c) hydraulic head along the channel and (d) evolution of outflux. MIN3P and TOUGHREACT data were taken from Xie et al. (2015) for comparison. For sub-plots a, b, and, c we collect the cell center data for *porousMedia4Foam*. For reference, we display the data at every 25 mm with a marker (black square). For MIN3P, the cell face data is plotted with the marker (red circle) displayed at every 25 mm. For TOUGHREACT, we digitize the data from plots available in Xie et al. (2015). 10Y refers to the data at time $t = 10$ years.

4.4 Results of case 4: Advective system subjected to porosity clogging - Calcite dissolution, gypsum precipitation/ dissolution and porosity feedback on permeability

The setup for this case was discussed in Section 3.4. Simulation results of *porousMedia4Foam*, MIN3P and TOUGHREACT for the evolution of porosity, gypsum and calcite volume fractions, hydraulic head, hydraulic conductivity along the column and also the outflux over time are plotted in Fig. 7.

All the results predicted by *porousMedia4Foam* at 10 years were in close agreement with MIN3P and TOUGHREACT. *porousMedia4Foam* predicted the porosity to reach minimum threshold value ($\phi = 0.001$) at 46 years at $x = 0.4625\,\mathrm{m}$ (distance from the inlet boundary). From this point of time, the reactive surface area of calcite and gypsum were considered to be minimal ($A_e = 10^{-6}\,\mathrm{m}^2/\mathrm{m}^3_{\mathrm{mineral}}$) in the control volume with minimal porosity threshold. This consideration prevented any further change in the volume fraction of minerals in specific control volumes. However, the porosity could still vary in the other control volumes surrounding the nearly clogged cell causing variation in flow within the column as reported by the outflux (Fig. 7f). In Xie et al. (2015), it was reported that other hydro-geochemical solvers reached a porosity of approximately 0.008 at 100 years and at 1000 years the porosity dropped to 0.001 approximately. We observed that the results of *porousMedia4Foam* in regard to the position along the column where porosity was minimal, presence of calcite dissolution front and maximum gypsum volume fraction, drop in hydraulic head and hydraulic conductivity were relatively close to the solutions of MIN3P and TOUGHREACT as seen in Fig. 7. The minor difference could potentially arise as some solvers used nodal data for analysis whereas *porousMedia4Foam* used cell centre data.

4.5 Results of case 5: An advective system with complex geochemical reactions and porosity feedback on permeability

The case setup for this benchmark was discussed in Section 3.5. The evolution of porosity, hydraulic head, hydraulic conductivity and outflux over time predicted by *porousMedia4Foam* compared with MIN3P and TOUGHREACT are plotted in Fig. 8. The evolution of all the mineral volume fractions obtained with *porousMedia4Foam* and compared with MIN3P, TOUGHREACT are plotted in Fig. 9. Overall, there was a good agreement between the results of *porousMedia4Foam*, MIN3P and TOUGHREACT. For this specific setup, gypsum (volume fraction of 0.45 at $x \approx 0.5\,\mathrm{m}$) majorly contributed in clogging the porous medium. A similar behaviour in the evolution of porosity with clogging occurring at approximately 0.5 m at 300 years (Fig. 8a) was observed for all the codes. *porousMedia4Foam* determined that the reactive system takes 164 years to reach the threshold porosity $\phi = 0.001$. Due to the clogging of the system, the hydraulic conductivity reduced to extremely low values as seen in Fig. 8c. The hydraulic head (Fig. 8b) determined by the solvers matched well at all times. There was a difference in the trend of the outflux determined by various solvers. Though for the first 50 years, all solvers predicted the same outflux, thereafter the results commenced to differ. This was the period from when the porosity fell to lower values and the outflux by then had already reduced by almost 99.9% from its initial values. A similar sort of behavior was also observed in Xie et al. (2015).

As seen in Fig. 9, we noticed a good match in the results determining the evolution of mineral volume fractions between *porousMedia4Foam* and other packages. An interesting observation was that of jarosite,

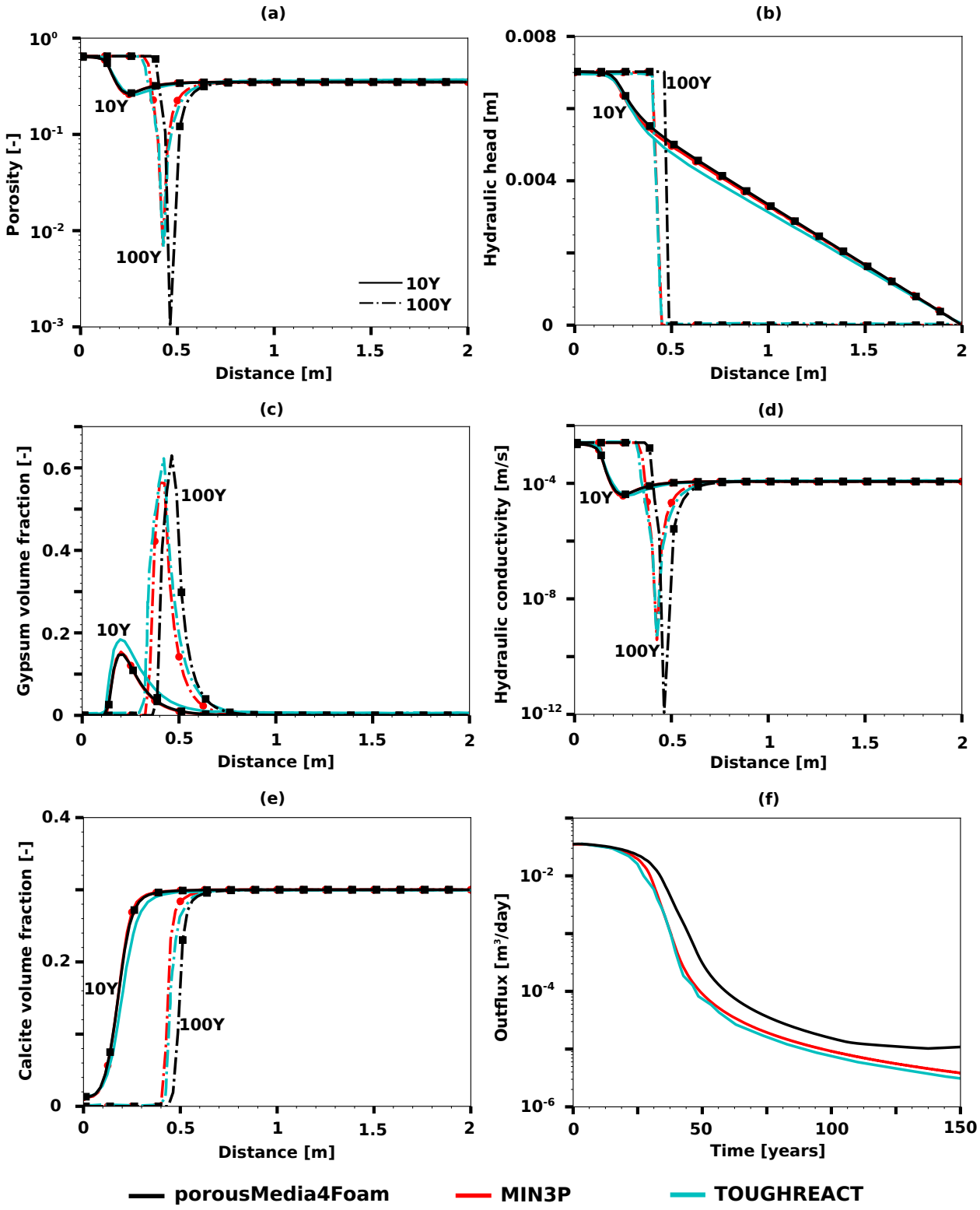


Figure 7: Case 4 - Calcite dissolution and gypsum precipitation/ dissolution under kinetic conditions considering feedback of porous media properties. Evolution of (a) porosity, (b) hydraulic head, (c) gypsum volume fraction, (d) hydraulic conductivity, (e) calcite volume fraction and (f) outflux. MIN3P and TOUGHREACT data were taken from Xie et al. (2015). For sub-plots a - e, we collect the cell center data for *porousMedia4Foam*. For reference, we display the data at every 25 mm with a marker (black square). For MIN3P, the cell face data is plotted with the marker (red circle) displayed at every 25 mm. For TOUGHREACT, we digitize the data from plots available in Xie et al. (2015). 10Y refers to the data at time $t = 10$ years.

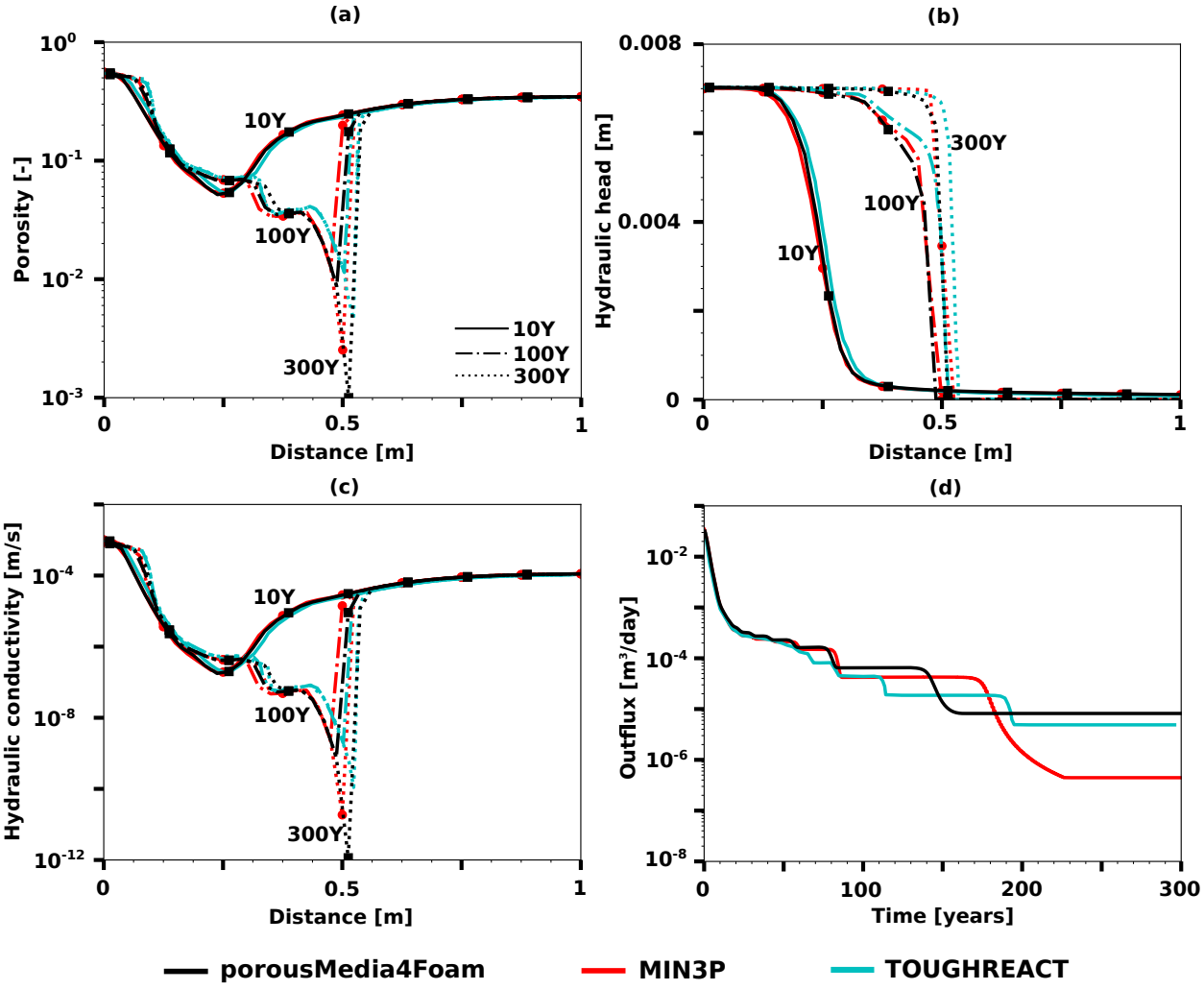


Figure 8: Case 5 – Evolution of (a) porosity, (b) hydraulic head, (c) hydraulic conductivity, and, (d) outflux over time. *porousMedia4Foam* results were compared with MIN3P and TOUGHREACT data taken from Xie et al. (2015). For subfigures (a), (b) and (c) the column length (represented on X-axis) had been scaled to 1 m to focus on the clogging zone.

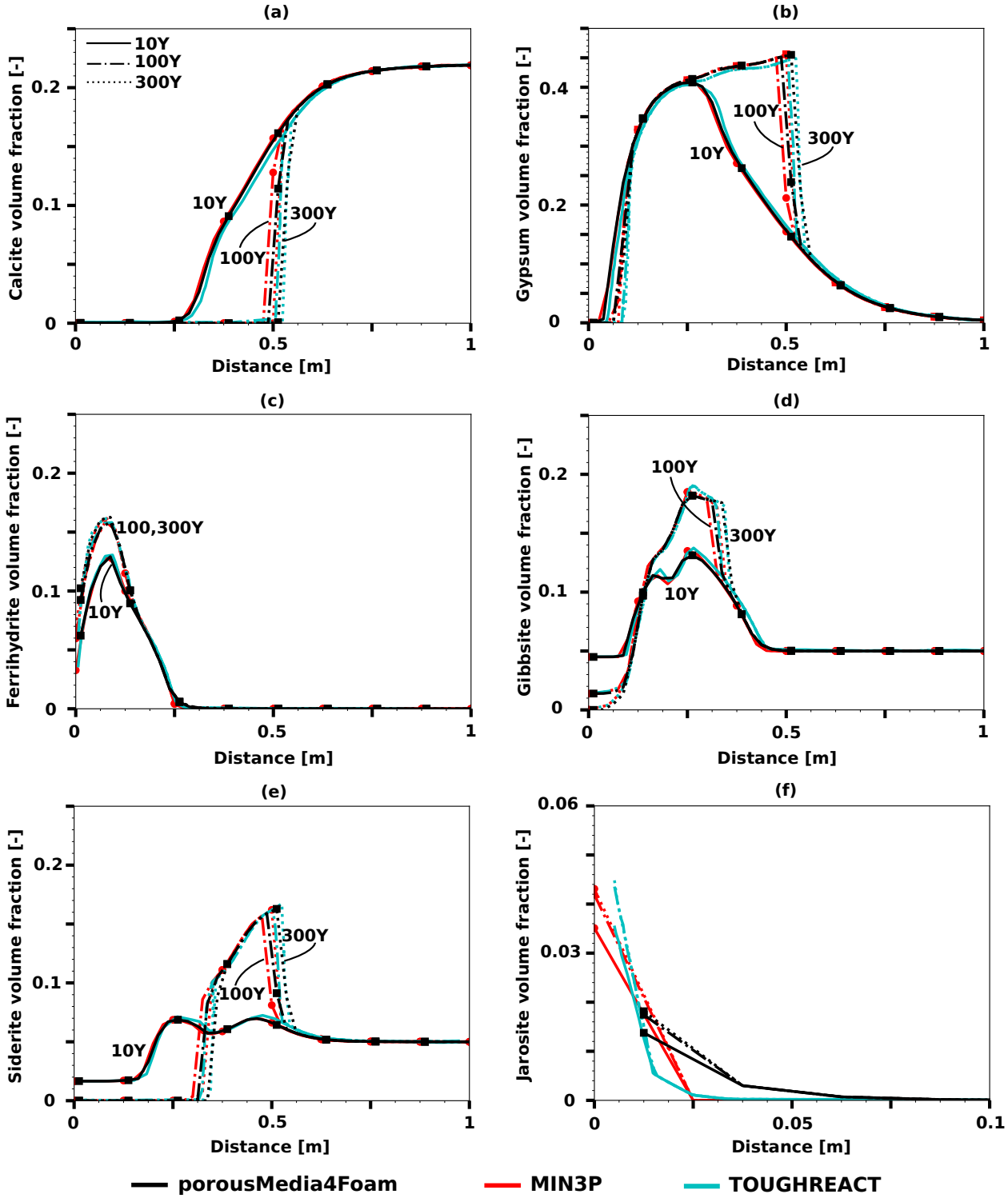


Figure 9: Case 5 – Evolution of various mineral volume fractions (a) calcite, (b) gypsum, (c) ferrihydrite, (d) gibbsite, (e) siderite, and, (f) jarosite. *porousMedia4Foam* results were compared with MIN3P and TOUGHREACT data taken from Xie et al. (2015). For subfigures (a) to (e) the column length (represented on X-axis) had been scaled to 1 m and for (f) the length had been scaled to 0.1 m. The scaling of the X-axis was done to focus on the region where minerals precipitated.

where *porousMedia4Foam* predicted approximately 50% less volume fraction compared to other solvers at 300 years (Fig. 9f). However, as seen in Fig. 9f, jarosite precipitated only near the inlet of the column.

4.6 Results of case 6: An advective-diffusive system with complex geochemical reactions and porosity feedback on permeability

The case setup for this benchmark was discussed in Section 3.6. The evolution of porosity, hydraulic head, hydraulic conductivity and outflux over time predicted by different reactive transport codes are shown in Fig. 10. Fig. 11 shows the evolution of various mineral volume fractions. The results of *porousMedia4Foam* were in good agreement with the results of MIN3P and TOUGHREACT. For this benchmark, *porousMedia4Foam* predicted that at 142 years, the geochemical system reached the threshold porosity at $x \approx 0.5\,\mathrm{m}$ – consistent with the clogging position determined by other solvers (Fig. 10a).

Likewise, the position of the hydraulic head front (Fig. 10b) and the position where the hydraulic conductivity was minimum (Fig. 10c) determined by *porousMedia4Foam* matched well with the solutions determined by other solvers. The determined outflux of all the solvers matched precisely up to 65 years (Fig. 10d). At 65 years, the outflux had already dropped by 99.9% from initial values. As the effect of clogging started to get prominent, the discrepancy in the predicted outflux between solvers started to show as we also observed in case 5 (Fig. 8d).

porousMedia4Foam determined that between 100 and 300 years, the precipitated gypsum (Fig. 11b) and gibbsite (Fig. 11d) close to the inlet dissolved more compared to the solution determined by other solvers. Just near the inlet, *porousMedia4Foam* predicted almost twice the amount of jarosite precipitate compared to the results of MIN3P and TOUGHREACT (Fig. 11f).

4.7 Results of case 7: A 2D advective-diffusive system with complex geochemical reactions and porosity feedback on permeability

The setup for this benchmark was discussed in Section 3.7. Fig. 12a shows the evolution of porosity at two specific points within the system – P1 (0.1, 1.0) and P2 (0.5, 1.0) – as represented in Fig. 2. Fig. 12b shows the evolution of outflux over a period of 300 years. P1 lies very close to the inlet boundary which could explain the different predictions obtained by all solvers. The evolution of porosity determined by various solvers at P2 was qualitatively consistent. The porosity at P2 dropped initially up to approximately 18 years and thereafter the porosity only marginally increased over time. From Fig. 12b we noticed that the outflux determined by different solvers were consistent for initial 20 years. From then on-wards, we noticed that the outflux determined by *porousMedia4Foam* was greater than other two solvers. At 20 years, the flux had already reduced by 96.5% from the initial value due to various minerals that precipitated all along the height of the channel at approximately $x = 0.5\,\mathrm{m}$ (see Fig. 13a for the distribution of porosity at 300 years).

Fig. 13 shows the porosity and permeability fields in the domain at 300 years. The porosity (Fig. 13a) was relatively high, $\phi \approx 0.5$ near the inlet and a substantial drop in porosity was observed in-between the region $x \approx 0.2\,\mathrm{m}$ to $x \approx 1\,\mathrm{m}$. Especially around $x \approx 1\,\mathrm{m}$, the porosity was substantially low, $\phi \approx 0.001$ which resulted in clogging of the system. Due to the decrease in porosity, the corresponding permeability also drastically reduced as shown in Fig. 13b.

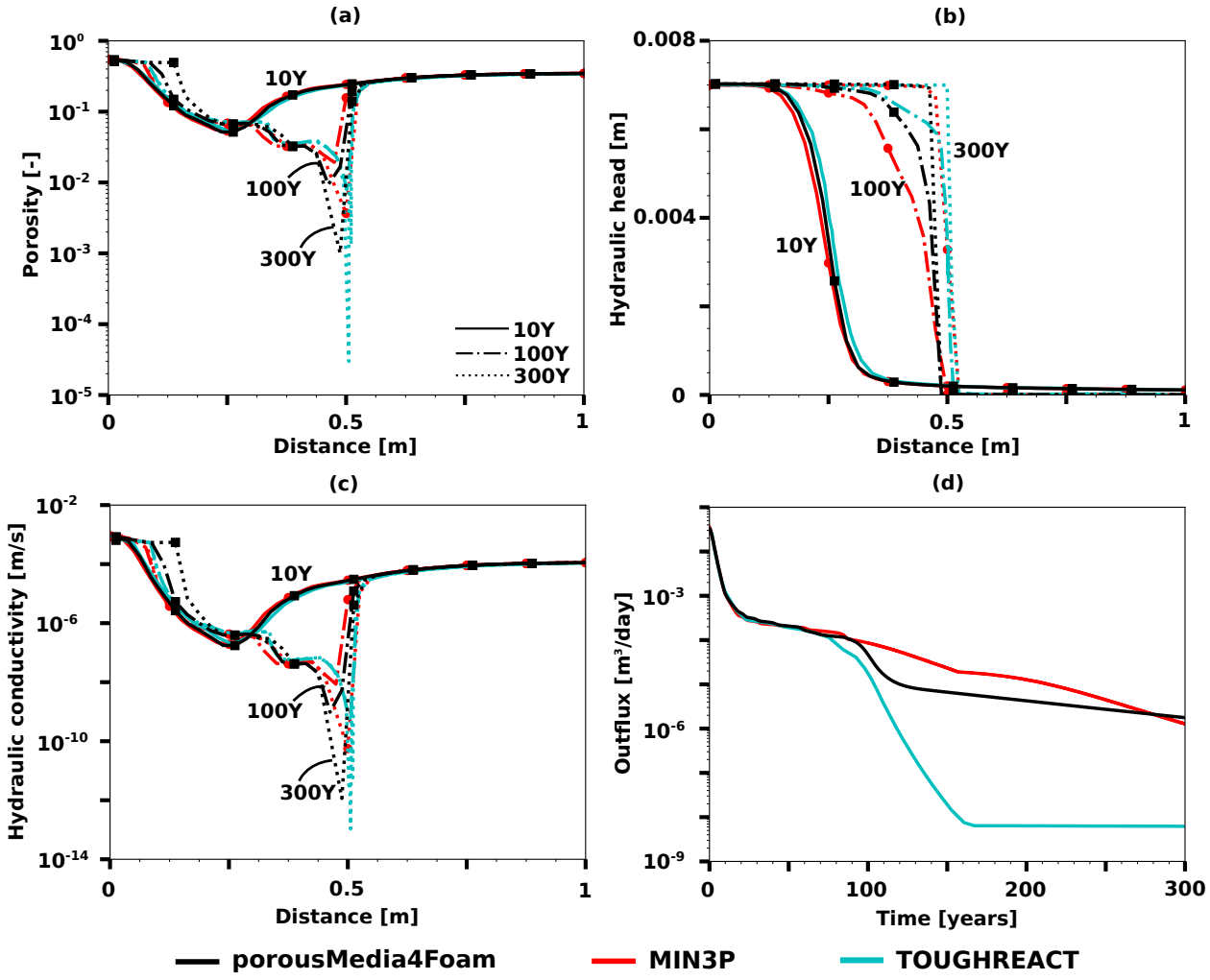


Figure 10: Case 6 – Evolution of (a) porosity, (b) hydraulic head, (c) hydraulic conductivity, and, (d) outflux over time for an advective-diffusive clogging system. *porousMedia4Foam* results were compared with MIN3P and TOUGHREACT results taken from Xie et al. (2015). For subfigures (a), (b), and, (c) the column length (represented on X-axis) had been scaled to 1 m to focus near the clogging zone.

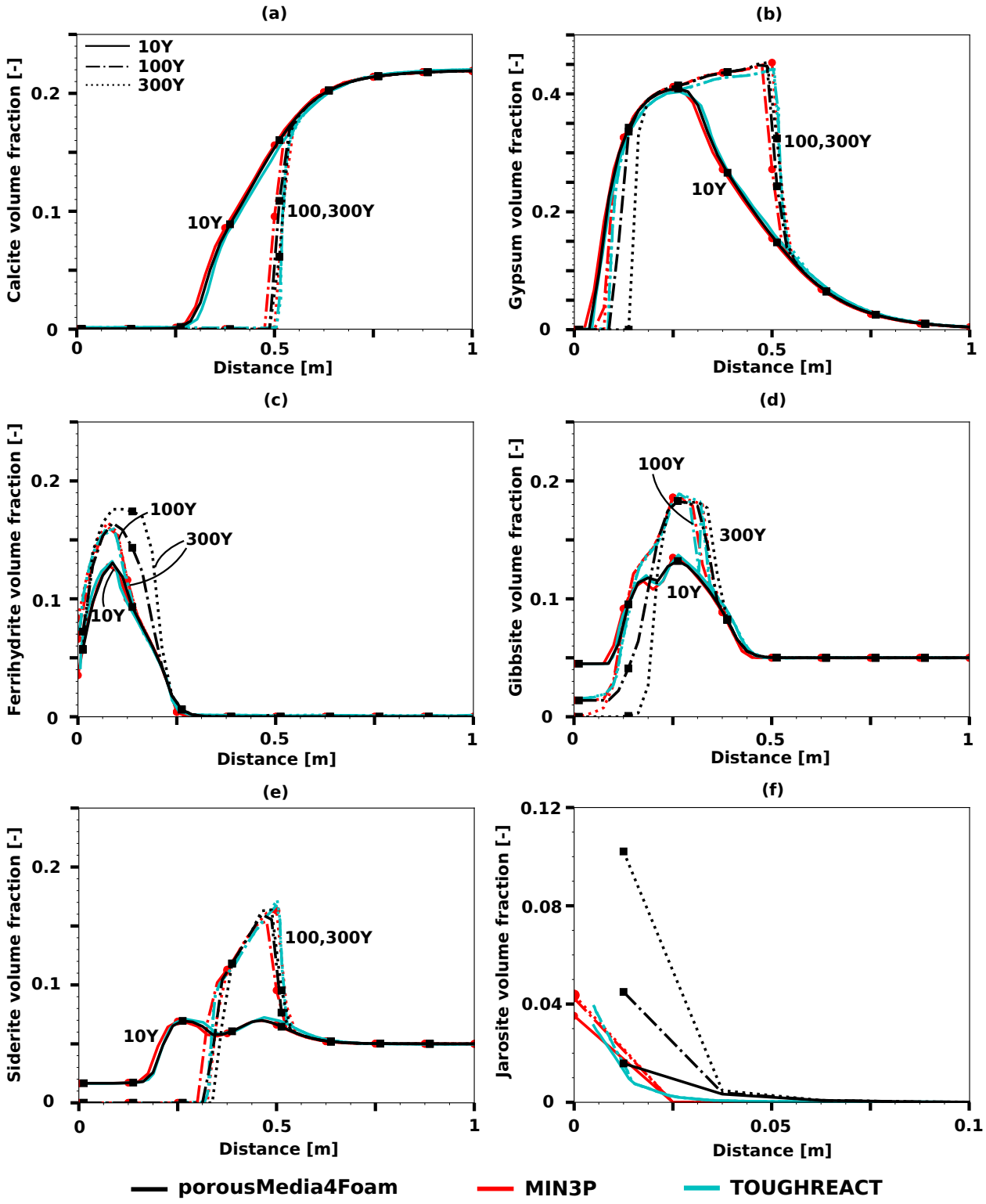


Figure 11: Case 6 – Evolution of various mineral volume fractions (a) calcite, (b) gypsum, (c) ferrihydrite, (d) gibbsite, (e) siderite, and, (f) jarosite in an advective-diffusive environment. *porousMedia4Foam* results were compared with MIN3P and TOUGHREACT data taken from Xie et al. (2015). For subfigures (a) to (e), the column length (represented on X-axis) had been scaled to 1 m and for (f) the length had been scaled to 0.1 m to focus the region where minerals precipitated.

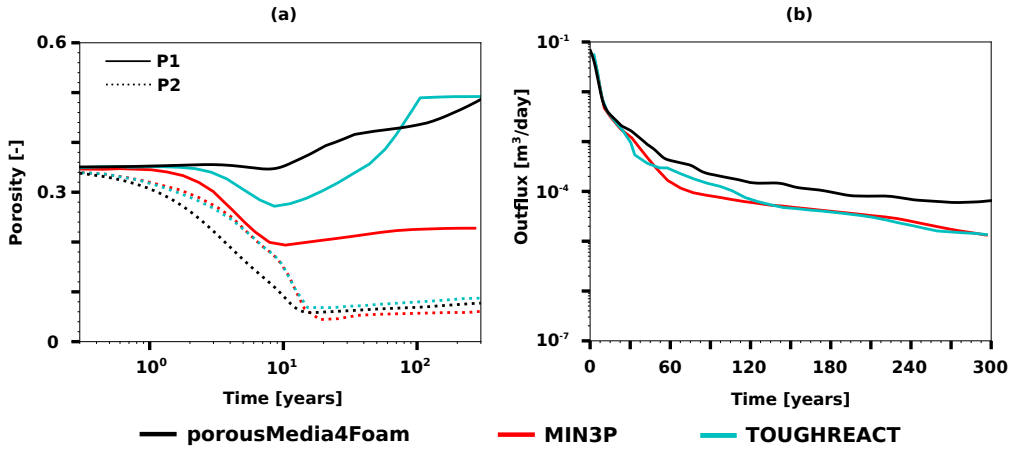


Figure 12: Case 7 – Comparison of results of *porousMedia4Foam* with MIN3P and TOUGHREACT data taken from Xie et al. (2015). Evolution of (a) porosity at points P1 and P2 as shown in Fig. 2, (b) outflux.

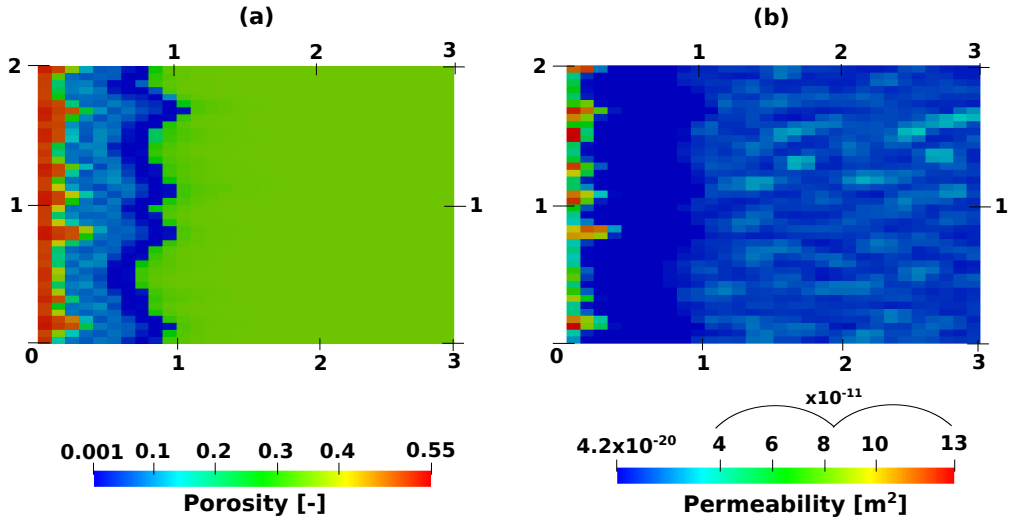


Figure 13: Case 7 - Results of *porousMedia4Foam* at 300 years. (a) Porosity, (b) permeability of the domain. Note that the scale used for permeability is different from the one shown in Fig. 2 for better visualisation.

4.8 Results of case 8: Reactive zone comprising of celestite having different grain sizes and considering porosity feedback on permeability

The setup for this benchmark was discussed in Section 3.8. Fig. 14 shows the mineral concentration of celestite (small grains, large grains and total) and barite within the flow cell after 300 hours. The results of *porousMedia4Foam* –with structured and unstructured mesh– were in very good agreement with the results obtained by TOUGHREACT and MIN3P in Poonoosamy et al. (2018). As smaller celestite grains had a larger reactive surface area in comparison to larger celestite grains, the ~~acidic~~ solution comprising of barium reacted with smaller celestite grains precipitating barite. Over 300 years, we noticed a substantial amount of smaller celestite grains that had dissolved and barite which had precipitated. The larger celestite grains, however, only had shown minimal amounts of dissolution.

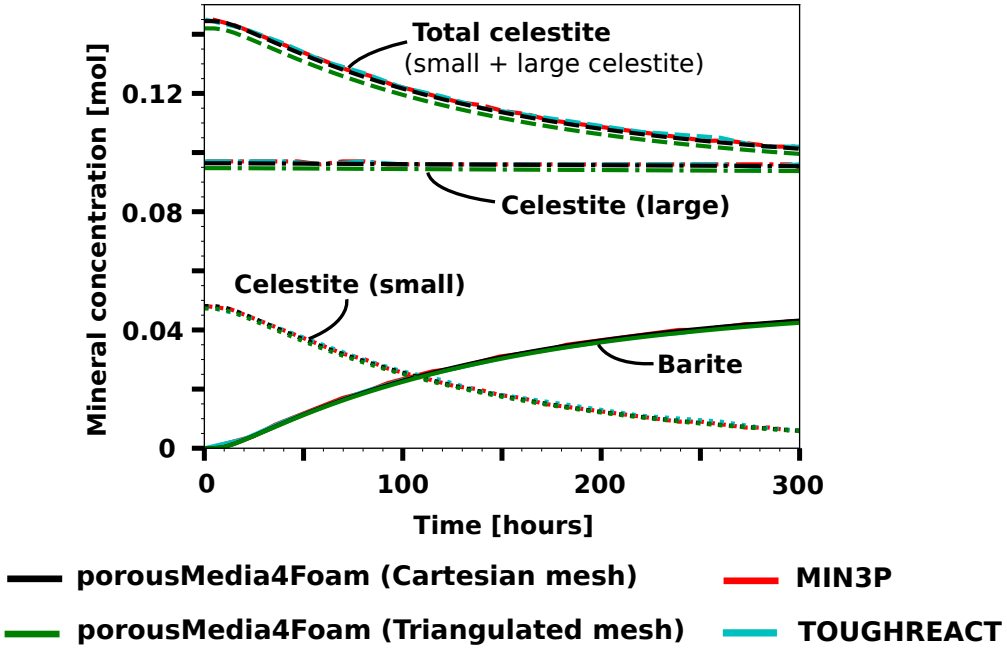


Figure 14: Case 8 – Concentration of celestite - small, large grains, total and barite in the flow cell after 300 hours. Results of *porousMedia4Foam* (with structured, unstructured mesh) was compared with the data obtained by TOUGHREACT and MIN3P from Poonoosamy et al. (2018).

Fig. 15 shows the results of porosity and permeability at 300 hours in the Q2 zone ($x = 0.045\,\text{m}$ to $x = 0.055\,\text{m}$). The data was collected at a heigth of $y = 0.01\,\text{m}$ in the flow cell. Within the Q2 zone, the porosity had reduced from an initial value of 0.33 to 0.305. Correspondingly, the permeability had decreased approximately by two orders of magnitude due to the precipitation of barite. *porousMedia4Foam* results were in good agreement with TOUGHREACT and MIN3P.

Fig. 16 compares the results of *porousMedia4Foam* with TOUGHREACT and MIN3P for the evolution of primary ion concentrations –barium (Ba^2+), chloride (Cl^-) and strontium (Sr^2+)– along the length of the flow cell at a height of $y = 0.01\,\text{m}$ at 150 hours (Fig. 16a) and 300 hours (Fig. 16b). Once again we noticed a good match between all solvers. At 150 years, as the process of dissolution of smaller celestite grains and barite precipitation was ongoing, the fronts of barium and strontium ions were relatively well-noticed

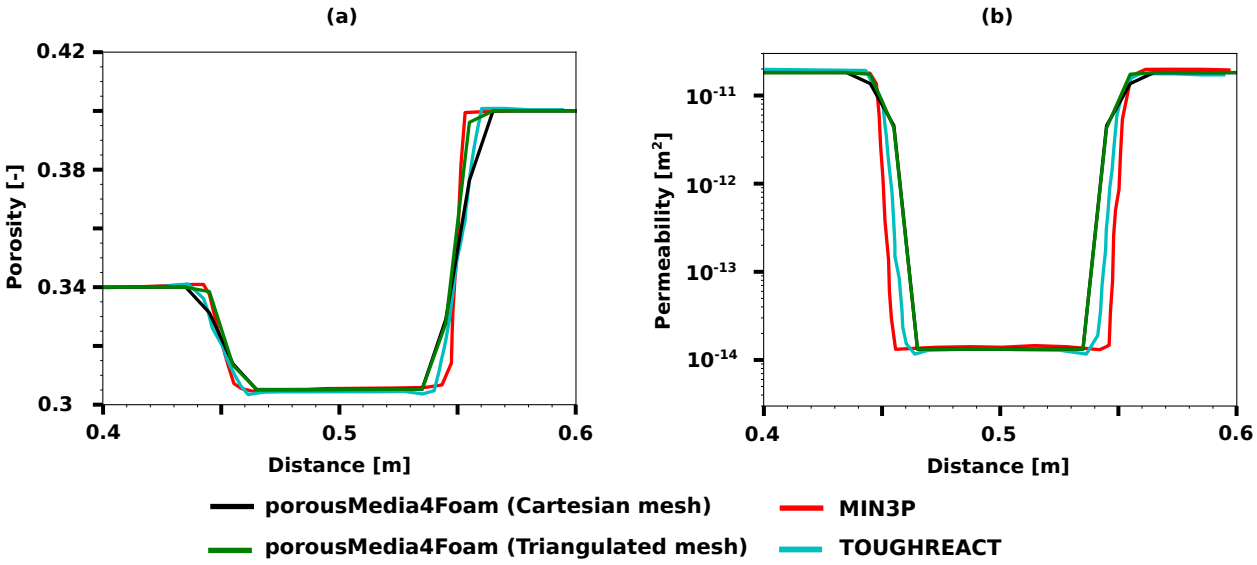


Figure 15: Case 8 – Change in porous media properties (a) porosity, (b) permeability at 300 hours due to dissolution of celestite and precipitation of barite in Q2 zone of the flow cell. The results of *porousMedia4Foam* were compared with TOUGHREACT and MIN3P which were taken from Poonoosamy et al. (2018).

compared to the concentration fronts of the same ions at 300 years. At 300 years, as significant amount of smaller grains had already dissolved and larger celestite grains reacted slowly with the incoming acidic solution, the front was not as sharp as seen at 150 years.

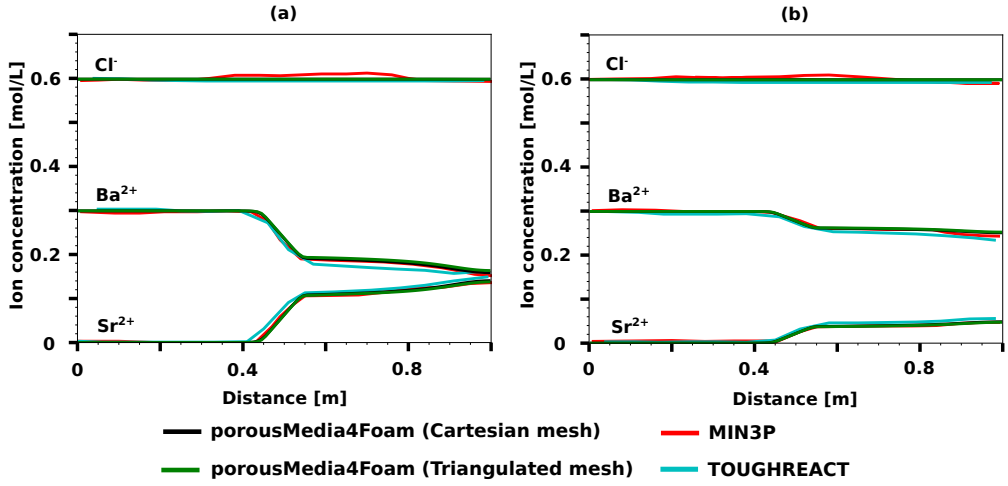


Figure 16: Case 8 – Evolution of the primary ion species –barium (Ba^{2+}), strontium (Sr^{2+}) and chloride (Cl^{-}) within the flow cell at (a) 150 hours, (b) 300 hours. The data was collected at a height of $y = 0.01\,\mathrm{m}$ along the length of the flow cell.

5 Conclusion

porousMedia4Foam is a new generation open-source multi-scale hydro-geochemical package developed by the authors that couples OpenFOAM® - a CFD package used to solve for the flow and transport of species, and PHREEQC - a geochemical package used to solve for chemical interactions.

In this numerical benchmark paper, we verified the robustness of the OpenFOAM-PHREEQC coupling by running eight cases of increasing complexity for which reference solutions exist. These solutions are well-established and used in the reactive transport community to benchmark the state-of-the-art reactive transport codes at the continuum-scale (Xie et al., 2015; Poonoosamy et al., 2018). The benchmarks included cases considering multiple minerals within the reactive environment that account for phase equilibrium and/or kinetic reactions both in one- and two-dimensional domains. The verification tests also involved complex feedback of porosity on transport properties including permeability and minerals reactive surface area. We also verified that our package could effectively handle reactive transport on unstructured meshes. We demonstrated that *porousMedia4Foam* successfully reproduced all the test cases which gave full confidence to use the simulation platform for predictive purposes or experiment modeling.

In addition to single phase reactive transport discussed in this manuscript, *porousMedia4Foam* comprises of extensive set of libraries and solvers that can also handle multi-phase reactive transport which is currently being validated. The flow solvers included in *porousMedia4Foam* embed two-phase Darcy's models using concepts such as relative permeabilities and capillary pressure. ~~Next, we will extend our hydro-geochemical simulator to model multi-phase flow processes in reactive environments.~~ At last but not least OpenFOAM is widely used in process engineering and its coupling with PHREEQC could be used beyond environmental geoscience application to account for (bio)chemical reactivity which is a key issue for the design, implementation, control, and optimisation of industrial processes.

Electronic Annex

The electronic annex to the manuscript comprises of the following: description of the injected solution, initial solution in the flow cell for benchmark 8, and, the computational architecture used for the benchmarks along with information related to the computational time and matrix solvers used.

Contributions of the authors

SP designed, setup the benchmark problems and ran simulations. CS is the architect of *porousMedia4Foam*. SP, CT and CS implemented new models in *porousMedia4Foam* and corrected bugs. SP, CT, FC and CS discussed, interpreted the results and wrote the paper. CS, CT and FC applied for funding.

Acknowledgements

The research leading to these results has received funding from the French Agency for Research (Agence Nationale de la Recherche, ANR) through the labex Voltaire ANR-10-LABX-100-01, the grant CATCH ANR-18-CE05-0035, and through the FraMatI project under contract ANR-19-CE05-0002. It has also received financial support from the CNRS through the MITI interdisciplinary programs. This project has received funding from the European Union's Horizon 2020 research and innovation programme under grant agreement

No 847593 (WP DONUT). SP postdoctoral fellowship was funded by BRGM through the PORE-REACTIF project from the Alliance Nationale de Coordination de la Recherche pour l'Energie (ANCRE). The authors benefitted from the use of the cluster at the Centre de Calcul Scientifique en région Centre-Val de Loire.

References

André, L., Audigane, P., Azaroual, M., and Menjoz, A. (2007). Numerical modeling of fluid–rock chemical interactions at the supercritical co2–liquid interface during co2 injection into a carbonate reservoir, the dogger aquifer (paris basin, france). *Energy conversion and management*, 48(6):1782–1797.

Archie, G. E. (1942). The electrical resistivity log as an aid in determining some reservoir characteristics. *Transactions of the AIME*, 146:54–62.

Aziz, K. (1979). Petroleum reservoir simulation. *Applied Science Publishers*, 476.

Bauer, S., Beyer, C., Dethlefsen, F., Dietrich, P., Duttmann, R., Ebert, M., Feeser, V., Görke, U., Köber, R., Kolditz, O., et al. (2013). Impacts of the use of the geological subsurface for energy storage: an investigation concept. *Environmental earth sciences*, 70(8):3935–3943.

Bea, S., Mayer, U., and MacQuarrie, K. (2016). Reactive transport and thermo-hydro-mechanical coupling in deep sedimentary basins affected by glaciation cycles: model development, verification, and illustrative example. *Geofluids*, 16:279–300.

Bear, J. (1972). *Dynamics of fluids in porous media*. Elsevier, New York.

Bildstein, O. and Claret, F. (2015). Chapter 5 - stability of clay barriers under chemical perturbations. In Tournassat, C., Steefel, C. I., Bourg, I. C., and Bergaya, F., editors, *Natural and Engineered Clay Barriers*, volume 6 of *Developments in Clay Science*, pages 155–188. Elsevier.

Bildstein, O., Claret, F., and Frugier, P. (2019). Rtm for waste repositories. *Reviews in Mineralogy and Geochemistry*, 85(1):419–457.

Carman, P. C. (1937). Fluid flow through granular beds. *Trans. Inst. Chem. Eng.*, 15:150–166.

Carrayrou, J., Mosé, R., and Behra, P. (2004). Operator-splitting procedures for reactive transport and comparison of mass balance errors. *Journal of Contaminant Hydrology*, 68(3-4):239–268.

Chagneau, A., Claret, F., Enzmann, F., Kersten, M., Heck, S., Madé, B., and Schäfer, T. (2015a). mineral precipitation-induced porosity reduction and its effect on transport parameters in diffusion-controlled porous media. *Geochemical transactions*, 16(1):1–16.

Chagneau, A., Tournassat, C., Steefel, C. I., Bourg, I. C., Gaboreau, S., Esteve, I., Kupcik, T., Claret, F., and Schäfer, T. (2015b). complete restriction of 36cl–diffusion by celestite precipitation in densely compacted illite. *Environmental Science & Technology Letters*, 2(5):139–143.

Claret, F., Marty, N., Tournassat, C., Xiao, Y., Whitaker, F., Xu, T., and Steefel, C. (2018). Modeling the long-term stability of multi-barrier systems for nuclear waste disposal in geological clay formations. *Reactive Transport Modeling: Applications in Subsurface Energy, and Environmental Problems. John Wiley & Sons, Ltd Chichester, UK*, pages 395–451.

Dake, L. P. (1983). *Fundamentals of reservoir engineering*. Elsevier.

Darcy, H. (1856). *Les fontaines publiques de la ville de Dijon: exposition et application...* Victor Dalmont.

DePaolo, D. J. and Cole, D. R. (2013). Geochemistry of geologic carbon sequestration: an overview. *Reviews in Mineralogy and Geochemistry*, 77(1):1–14.

Druhan, J., Tournassat, C., et al. (2020). *Reactive Transport in Natural and Engineered Systems*, volume 85. Walter de Gruyter GmbH & Co KG.

Gaus, I., Audigane, P., André, L., Lions, J., Jacquemet, N., Durst, P., Czernichowski-Lauriol, I., and Azaroual, M. (2008). Geochemical and solute transport modelling for co2 storage, what to expect from it? *International journal of greenhouse gas control*, 2(4):605–625.

Haszeldine, R. S. (2009). Carbon capture and storage: how green can black be? *Science*, 325(5948):1647–1652.

Heinemann, N., Alcalde, J., Miocic, J. M., Hangx, S. J., Kallmeyer, J., Ostertag-Henning, C., Hassanpouryouzband, A., Thaysen, E. M., Strobel, G. J., Schmidt-Hattenberger, C., et al. (2021). Enabling large-scale hydrogen storage in porous media–the scientific challenges. *Energy & Environmental Science*.

Horgue, P., Soulaine, C., Franc, J., Guibert, R., and Debenest, G. (2015). An open-source toolbox for multiphase flow in porous media. *Computer Physics Communications*, 187(0):217– 226.

Kozeny, J. (1927). Uber kapillare leitung der wasser in boden. *Royal Academy of Science, Vienna, Proc. Class I*, 136:271–306.

Lackner, K. S. (2003). A guide to co2 sequestration. *Science*, 300(5626):1677–1678.

Landais, P. (2006). Advances in geochemical research for the underground disposal of high-level, long-lived radioactive waste in a clay formation. *Journal of Geochemical Exploration*, 88(1-3):32–36.

Lichtner, P. C., Hammond, G. E., Lu, C., Karra, S., Bisht, G., Andre, B., Mills, R., and Kumar, J. (2015). Pflotran user manual: A massively parallel reactive flow and transport model for describing surface and subsurface processes. Technical report, Los Alamos National Lab.(LANL), Los Alamos, NM (United States); Sandia ....

Luhmann, A., Tutolo, B. M., Bagley, B., Mildner, D., Seyfried, W., and Saar, M. (2017). Permeability, porosity, and mineral surface area changes in basalt cores induced by reactive transport of co2-rich brine. *Water Resources Research*, 53:1908–1927.

Mayer, K. U., Frind, E. O., and Blowes, D. W. (2002a). Multicomponent reactive transport modeling in variably saturated porous media using a generalized formulation for kinetically controlled reactions. *Water Resources Research*, 38(9):13–1.

Mayer, K. U., Frind, E. O., and Blowes, D. W. (2002b). Multicomponent reactive transport modeling in variably saturated porous media using a generalized formulation for kinetically controlled reactions. *Water Resources Research*, 38(9):13–1.

Min, T., Gao, Y., Chen, L., Kang, Q., and Tao, W. (2015). Changes in porosity, permeability and surface area during rock dissolution: effects of mineralogical heterogeneity. *arXiv: Fluid Dynamics*.

Molins, S., Soulaine, C., Prasianakis, N., Abbasi, A., Poncet, P., Ladd, A., Starchenko, V., Roman, S., Trebotich, D., Tchelepi, H., and Steefel, C. (2020). Simulation of mineral dissolution at the pore scale with evolving fluid-solid interfaces: Review of approaches and benchmark problem set. *Computational Geosciences*, pages 1–34.

Niu, Q. and Zhang, C. (2019). Permeability prediction in rocks experiencing mineral precipitation and dissolution: A numerical study. *Water Resources Research*, 55:3107–3121.

Noiriel, C. (2015). Resolving time-dependent evolution of pore-scale structure, permeability and reactivity using x-ray microtomography. *Reviews in Mineralogy and Geochemistry*, 80(1):247–285.

Noiriel, C. and Daval, D. (2017). Pore-scale geochemical reactivity associated with co2 storage: New frontiers at the fluid-solid interface. *Accounts of chemical research*, 50 4:759–768.

Noiriel, C., Steefel, C., Yang, L., and Bernard, D. (2016). Effects of pore-scale precipitation on permeability and flow. *Advances in Water Resources*, 95:125–137.

Parkhurst, D. and Appelo, C. (2013). Description of input and examples for phreeqc version 3: a computer program for speciation, batch-reaction, one-dimensional transport, and inverse geochemical calculations. *Techniques and Methods*.

Parkhurst, D. L. and Wissmeier, L. (2015). PhreeqcRM: A reaction module for transport simulators based on the geochemical model PHREEQC. *Advances in Water Resources*, 83:176–189.

Pavuluri, S. (2019). *Direct numerical simulations of spontaneous imbibition at the pore-scale: impact of parasitic currents and dynamic capillary barriers*. PhD thesis, Heriot-Watt University.

Poonoosamy, J., Soulaine, C., Burmeister, A., Deissmann, G., Bosbach, D., and Roman, S. (2020). Microfluidic flow-through reactor and 3d raman imaging for in situ assessment of mineral reactivity in porous and fractured porous media. *Lab on a Chip*, 20(14):2562–2571.

Poonoosamy, J., Wanner, C., Alt Epping, P., Águila, J. F., Samper, J., Montenegro, L., Xie, M., Su, D., Mayer, K. U., Mäder, U., Van Loon, L. R., and Kosakowski, G. (2018). Benchmarking of reactive transport codes for 2d simulations with mineral dissolution–precipitation reactions and feedback on transport parameters. *Computational Geosciences*, pages 1–22.

Soulaine, C., Maes, J., and Roman, S. (2021a). Computational microfluidics for geosciences. *Frontiers in Water*, 3:11.

Soulaine, C., Pavuluri, S., Claret, F., and Tournassat, C. (2021b). porousmedia4foam: Multi-scale open-source platform for hydro-geochemical simulations with openfoam. *Earth and Space Science Open Archive ESSOAr*.

Soulaine, C., Roman, S., Kovscek, A., and Tchelepi, H. (2018). Pore-scale modelling of multiphase reactive flow: application to mineral dissolution with production of. *Journal of Fluid Mechanics*, 855:616–645.

Soulaine, C., Roman, S., Kovscek, A., and Tchelepi, H. A. (2017). Mineral dissolution and wormholing from a pore-scale perspective. *Journal of Fluid Mechanics*, 827:457–483.

Soulaine, C. and Tchelepi, H. (2016). Micro-continuum approach for pore-scale simulation of subsurface processes. *Transport in Porous Media*, 113:431–456.

Steefel, C., Appelo, C., Arora, B., Jacques, D., Kalbacher, T., Kolditz, O., Lagneau, V., Lichtner, P., Mayer, K. U., Meeussen, J., et al. (2015). Reactive transport codes for subsurface environmental simulation. *Computational Geosciences*, 19(3):445–478.

Steefel, C. I. (2009). Crunchflow. *Software for modeling multicomponent reactive flow and transport. User's manual. Lawrence Berkeley National Laboratory, Berkeley.*

Steefel, C. I. (2019). Reactive transport at the crossroads. *Reviews in Mineralogy and Geochemistry*, 85(1):1–26.

Steefel, C. I., DePaolo, D. J., and Lichtner, P. C. (2005). Reactive transport modeling: An essential tool and a new research approach for the earth sciences. *Earth and Planetary Science Letters*, 240(3-4):539–558.

Strang, G. (1968). On the construction and comparison of difference schemes. *SIAM Journal on Numerical Analysis*, 5(3):pp. 506–517.

Su, D., Mayer, K. U., and MacQuarrie, K. T. (2020). Min3p-hpc: A high-performance unstructured grid code for subsurface flow and reactive transport simulation. *Mathematical Geosciences*, pages 1–34.

Thoenen, T., Hummel, W., Berner, U., and Curti, E. (2014). The psi/nagra chemical thermodynamic database 12/07.

Tournassat, C. and Steefel, C. I. (2019). Reactive Transport Modeling of Coupled Processes in Nanoporous Media. *Reviews in Mineralogy and Geochemistry*, 85(1):75–109.

Trebotich, D., Adams, M. F., Molins, S., Steefel, C. I., and Shen, C. (2014). High-resolution simulation of pore-scale reactive transport processes associated with carbon sequestration. *Computing in Science & Engineering*, 16(6):22–31.

Xie, M., Mayer, K. U., Claret, F., Alt-Epping, P., Jacques, D., Steefel, C., Chiaberge, C., and Simunek, J. (2015). Implementation and evaluation of permeability-porosity and tortuosity-porosity relationships linked to mineral dissolution-precipitation. *Computational geosciences*, 19(3):655–671.

Xu, T., Spycher, N., Sonnenthal, E., Zhang, G., Zheng, L., and Pruess, K. (2011). Toughreact version 2.0: A simulator for subsurface reactive transport under non-isothermal multiphase flow conditions. *Computers & Geosciences*, 37(6):763–774.

Zhang, R., Yin, X., Winterfeld, P. H., and Wu, Y.-S. (2016). A fully coupled thermal-hydrological-mechanical-chemical model for co2 geological sequestration. *Journal of Natural Gas Science and Engineering*, 28:280–304.